Neutron star mergers as the cause for the variance in Xe distribution in the Solar System

A dissertation submitted to The University of Manchester for the degree of

Master of Science by Research

in the Faculty of Science and Engineering

Year of submission

2021

Student ID

10803915

School of Natural Sciences

Department of Physics and Astronomy

Contents

Word count: 10097

3

List of figures

List of tables

Abstract

Xenon has nine stable isotopes. However, the relative populations of these isotopes vary between various sources across the Solar System. Of note, is the difference between the xenon composition of the solar wind and the xenon composition of the comets.

This heterogeneity can be caused by variation in the nucleosynthesis of the xenon. Xenon is made from two nucleosynthetic routes: the r- and s-process. The s-process occurs when the rate of neutron addition is slower than the β-decay. The r-process occurs when the rate of neutron addition is faster than the rate of β-decay. The products of the s-process can be calculated and, thus, subtracted from the measured compositions.

Once the s-process is removed, the remainder is considered to be from the r-process. By comparing the r-process compositions there is evidence of multiple r-processes contributing to the Solar System. Specifically, the xenon abundances are hard to reconcile with yields from a single uniform source of r-process elements.

This paper considers neutron star mergers as the source of one of these r-processes. A model was used to consider the evolution of r-process matter in the Galaxy due to the neutron star mergers. In the model, the rotation of the Galaxy and the diffusion of matter through the interstellar matter was considered.

Through this model, it was found that local conditions in only 1.3% of the Galaxy are consistent with the cometary and Solar xenon compositions. This suggests that the xenon composition of the Solar System is rare among solar systems that form in the Galaxy. Based on this, the effects of various simplifications and assumptions used to make the model were examined.

Declaration of originality

I hereby confirm that this dissertation is my own original work unless referenced clearly to the contrary, and that no portion of the work referred to in the dissertation has been submitted in support of an application for another degree or qualification of this or any other university or other institute of learning.

Intellectual property statement

i The author of this thesis (including any appendices and/or schedules to this thesis) owns certain copyright or related rights in it (the "Copyright") and s/he has given The University of Manchester certain rights to use such Copyright, including for administrative purposes.

ii Copies of this thesis, either in full or in extracts and whether in hard or electronic copy, may be made *only* in accordance with the Copyright, Designs and Patents Act 1988 (as amended) and regulations issued under it or, where appropriate, in accordance with licensing agreements which the University has from time to time. This page must form part of any such copies made.

iii The ownership of certain Copyright, patents, designs, trademarks and other intellectual property (the "Intellectual Property") and any reproductions of copyright works in the thesis, for example graphs and tables ("Reproductions"), which may be described in this thesis, may not be owned by the author and may be owned by third parties. Such Intellectual Property and Reproductions cannot and must not be made available for use without the prior written permission of the owner(s) of the relevant Intellectual Property and/or Reproductions.

iv Further information on the conditions under which disclosure, publication and commercialisation of this thesis, the Copyright and any Intellectual Property and/or Reproductions described in it may take place is available in the University IP Policy (see `http://documents.manchester.ac.uk/DocuInfo.aspx?DocID=24420`), in any relevant Dissertation restriction declarations deposited in the University Library, and The University Library's regulations (see `http://www.library.manchester.ac.uk/about/regulations/_files/Library-regulations.pdf`).

Acknowledgements

I would like to thank the invaluable help and guidance given to me by Prof. Albert Zijlstra and Prof. Jamie Gilmour.

1 Introduction

1.1 Background and motivation

Of all the chemical elements that exist today, only H, He, and Li were formed by the Big Bang (big-bang nucleosynthesis). The process by which the heavier elements form is called stellar nucleosynthesis. It acts in a dense plasma at temperatures high enough to overcome the Coulomb barrier between free protons. This happens at temperatures around 10^9 K (100 keV). The process forms helium and trace amounts of lithium. Heavier elements are not formed, for two reasons. First, the temperature drops rapidly and free neutrons have a half-life of roughly 10 min[1]; second, all nuclei with mass number $A = 5$ or $A = 8$, which result from fusing hydrogen with helium or helium with helium, are highly unstable. These form additional obstacles to building up heavier elements which the conditions at the Big Bang cannot overcome. At the end of Big Bang nucleosynthesis, the Universe contained 90% hydrogen and 10% helium, where densities are by number.

All other elements are made in stars. The first stars formed when the Universe was a few hundred million years old. Stars contain cores which have high density and very high temperatures. These conditions facilitate fusion. Stars generate energy primarily by fusing hydrogen to helium (by several possible routes depending on internal temperature and pressure)[1]. The temperature inside stars like the Sun is on the order of 10^7 K. At these temperatures, hydrogen fusion proceeds extremely slowly. In the Sun, a particular proton can wait for 10^{10} yr before it undergoes fusion. These hydrogen burning stars are within the main sequence, where a given star will spend the majority of its lifetime. In figure 1, the main sequence can be identified as the line of stars which stretch from hot and luminous to cool and dim.

As stars age, they run out of hydrogen in the core and switch to helium burning. In high mass stars, because of the increased density, helium burning can proceed through what is known as the triple-α process[3]. In the triple-α process, a population of ^{8}Be is maintained through α-particles combining and then decaying. This ^{8}Be is then impacted by another α-particle to make ^{12}C. This releases enough energy to overcome the bottleneck at $A = 8$. As the core successively runs out of nuclear fuel, the star will switch to burning heavier and heavier elements. Compared to hydrogen burning, helium burning produces much less energy per kilogram. This is even more so for the heavier elements. This means that the lifetime of each subsequent burning phase lasts for a shorter and shorter time. These later burning phases occur only in the largest stars and only occur in red giant and supergiant stars (Fig. 1).

All these products from nuclear burning are trapped within the cores of the stars. They are dispersed into the interstellar medium (ISM) when the stars die. There are two different ways in which

---

[1]This is only true for main-sequence stars. Giant branch star primarily generate energy through more advanced nuclear burning for example by fusing helium to carbon and oxygen
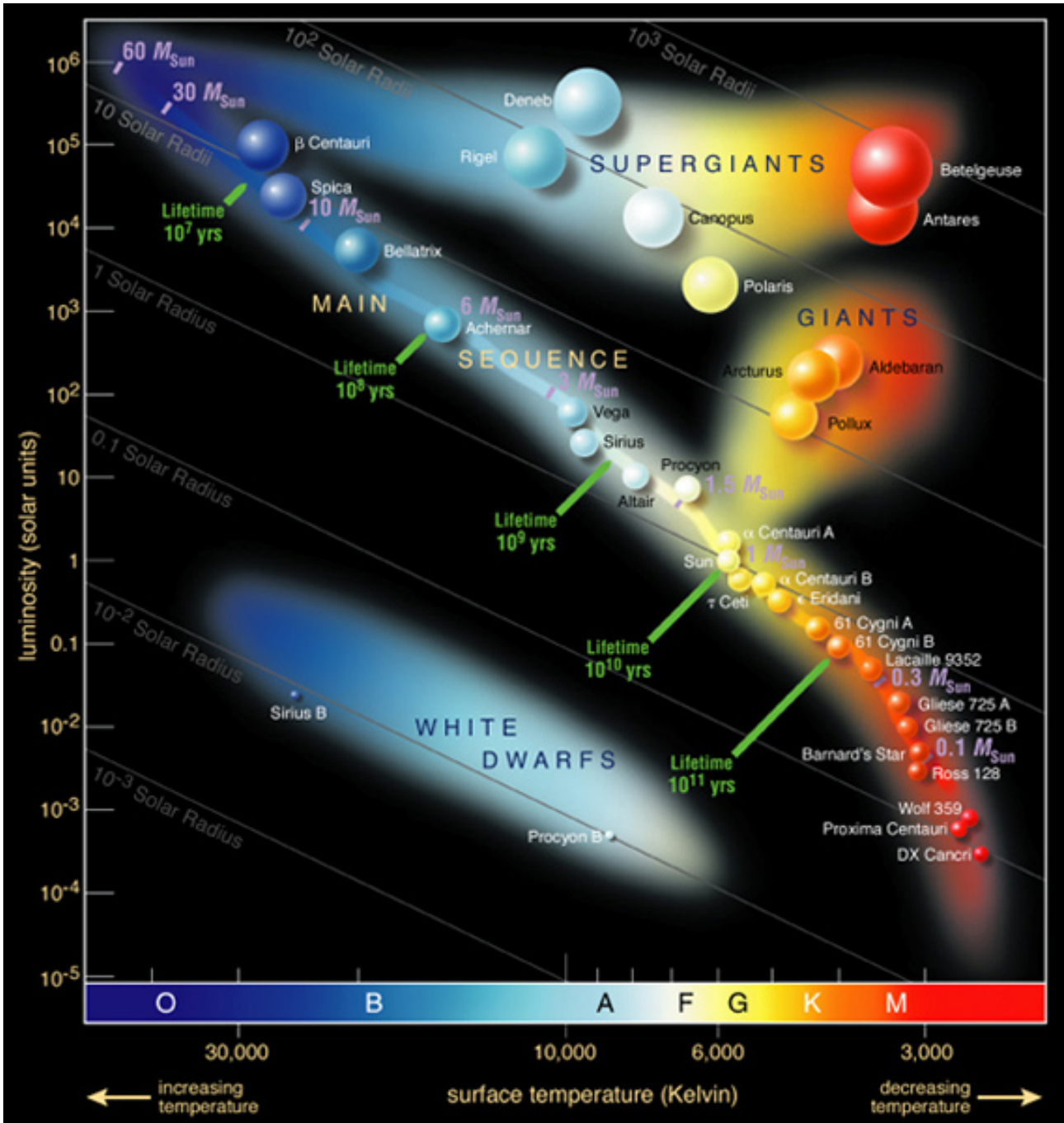
Fig. 1. *Hertzsprung-Russell diagram that plots temperature (in Kelvin) of stars against luminosity (in solar units). The main sequence is the line of stars running diagonally from bottom right to top left. Also note the giant branch and the supergiant branch. Adapted from ESO image archives[2]*

the matter is dispersed: one for low mass stars ($< 10\,M_\odot$[2]), and one for high mass stars ($> 10\,M_\odot$). For low mass stars, the core elements are brought to the surface by convection in the outer regions where they are then expelled through stellar wind. This happens on the asymptotic giant branch (AGB), which happens at a late phase in the evolution of the star. For high mass stars, majority of matter is ejected violently at the end of the stars life in a supernova explosion.

In this way, the interstellar medium becomes slowly enriched in the heavier elements. New stars form from the interstellar medium, and therefore these new generations of stars will start out with a larger fraction of heavier elements[3].

The nuclear fusion occurring within the stars is not enough to produce all elements. This is because, as can be seen in fig. 2, the binding energy per nucleon starts decreasing after iron. This means that making heavier nucleons is no longer an energy-positive process, resulting in a build up of iron in the cores of very massive stars. In addition to this increasing energy cost, there is a further barrier (in the form of the electric charge of the nucleons) with producing very heavy nucleons. This Coulomb barrier can be avoided by using adding electrically neutral neutrons to the nucleons. This works by impacting the nucleon with a neutron which becomes incorporated into the nucleon. If the new nucleon is unstable it will undergo β-decay (sometimes many times successively) to become a stable nucleon[4]. From this description, it can be seen that this neutron addition process requires environments with a significant excess of neutrons. Such environments occur during the AGB phase of stars and during stellar explosions.

The Solar System formed from the interstellar material 4.6 Gyr ago. Therefore, the composition of the Solar System reflects the state of enrichment of the ISM at the time of formation. This enrichment can be measured by observing isotope composition of the Sun. In addition, the composition of meteorites and comets provides another glimpse into the ISM at the Solar System's formation. Meteorites contain mainly refractory elements (e.g. Si, Fe, Al, Ca) while volatile (K, As, Sn) and extremely volatile elements (H, He, Ne, Xe) only occur in trace amounts. Comets, however, have a higher concentrations of volatile elements. Comets and meteorites are especially useful as they do not experience significant heating since their formation, which means that their original isotopic compositions are preserved.

These different traces of the Solar System's origin do not give identical abundances. This has three possible explanations: 1) the ISM that formed the Solar System was inhomogeneous and maintained this inhomogeneity within the Solar System, 2) the inhomogeneity formed from processes within the Solar System leading to separation among the elements, 3) the inhomogeneity occured from an enrichment event during the formation as the formation took some time.

There are many elements that display such isotopic heterogeneity, such as chromium[5] and oxygen[6][7]. This thesis will focus on the inhomogeneity in the isotopes of Xe throughout the Solar

---

[2] $M_\odot$ is the mass of the Sun

[3] known as metallicity

[4] β-decay transforms one neutron in the nucleon to a proton and releases an electron. This has the effect of maintaining the atomic weight and increasing the atomic number by one.
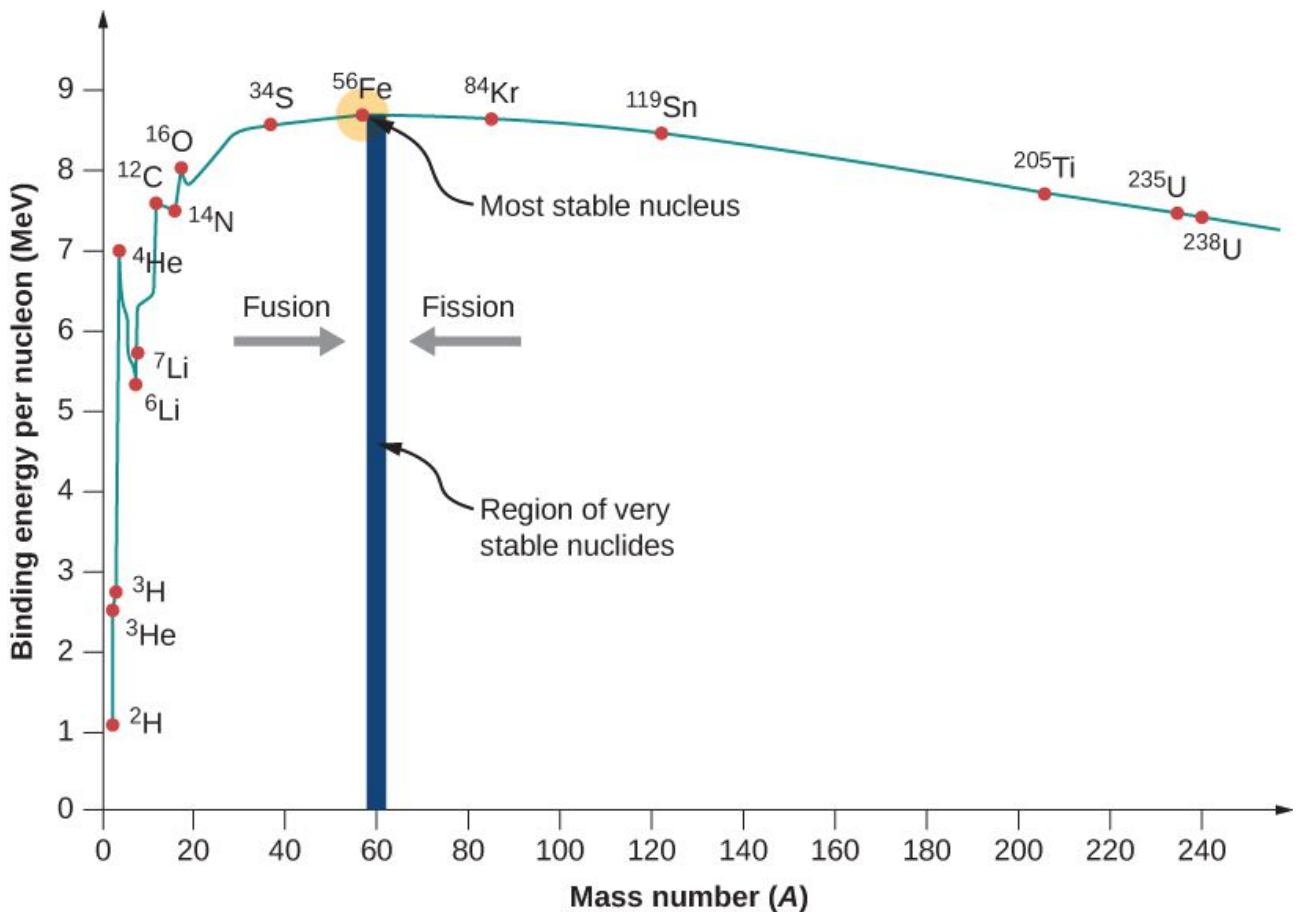
Fig. 2. *This diagram shows the mass number of the elements plotted against their binding energy per nucleon. Note that iron has the most binding energy per nucleon. Also note the decrease in energy difference as you go from hydrogen to iron. This means that less energy is released in stars that make heavier elements. This is the reason for older stars tend to cool as they age.[4]*

System. The isotopic ratios vary by 20%[8] between the different components of the Solar System. Due to xenon's high nuclear charge, it is mainly produced through neutron capture. In this thesis, I will study the possibility that the Solar System was enriched by a late addition of xenon from a different stellar source of neutron capture elements.

1.2 Aims and objectives

This paper will explore the likelihood that the Solar System during its formation was enriched by a neutron star merger. This late injection could then lead to the heterogeneity found between the modern Xe-SW and Xe-67P/CG compositions.

This is explored through a diffusion model of the Galaxy. The model follows the evolution of the Galaxy while neutron star mergers occur at random locations. After each neutron star merger, ejecta is diffused across the Galaxy and the amount of NSM matter is tracked over time for each location. The model uses both the rate of diffusion and the rotation of the Galaxy to spread material around.

The model is used to calculate the fractional change over a small time as a function of the galactic age and position. This can be compared to the Solar System's time of formation and duration of formation. The model provides a probability curve for the possible fractional changes in the xenon composition over a certain time. This is then compared to the fractional change derived from comparing measurements of Xe-SW and Xe-67P/CG.

1.3 Report structure

This report concerns a model of the Milky Way and from this estimates the frequency of stars with xenon compositions matching the Solar System's. The first part of the report will go over the background details regarding xenon, its origins and its compositions. Then it will cover the model used in the report and explain and justify the decisions made regarding it. Finally, the results from the model will be discussed and possible conclusions will be drawn. In addition, limitations and possible sites for future work will be covered in this final section.

2 Literature review

2.1 Neutron capture processes

Due to the growing Coulomb repulsion at higher nuclear charge, heavy elements are mainly made through neutron addition. Depending on the concentration of energetic neutrons in the environment there are two main processes through which the neutrons are added. The slow neutron capture process (known as s-process) occurs at low neutron concentrations. At high neutron concentrations, the rapid neutron capture process (r-process) occurs.

During the s-process, the neutron capture occurs slow enough that the resultant nuclei never stray far from the line of stability. The r-process, however, results in nuclei that are strongly enriched in neutron. These nuclei then decay to their most stable decay product.

2.1.1 S-process

The s-process adds neutrons slower than the unstable nuclei decay. This means that the produced nucleus will step along stable nuclei until an unstable nucleus in reached at which point β decay will occur.

On the nuclide chart in figure 4, the s-process will start from the bottom left with ^{116}Sn. Then neutrons are sequentially added to the nucleus moving the position on the chart to the right till ^{120}Sn is reached. When a further neutron is added to make ^{121}Sn, the nucleus β decays to ^{121}Sb. Similarly,
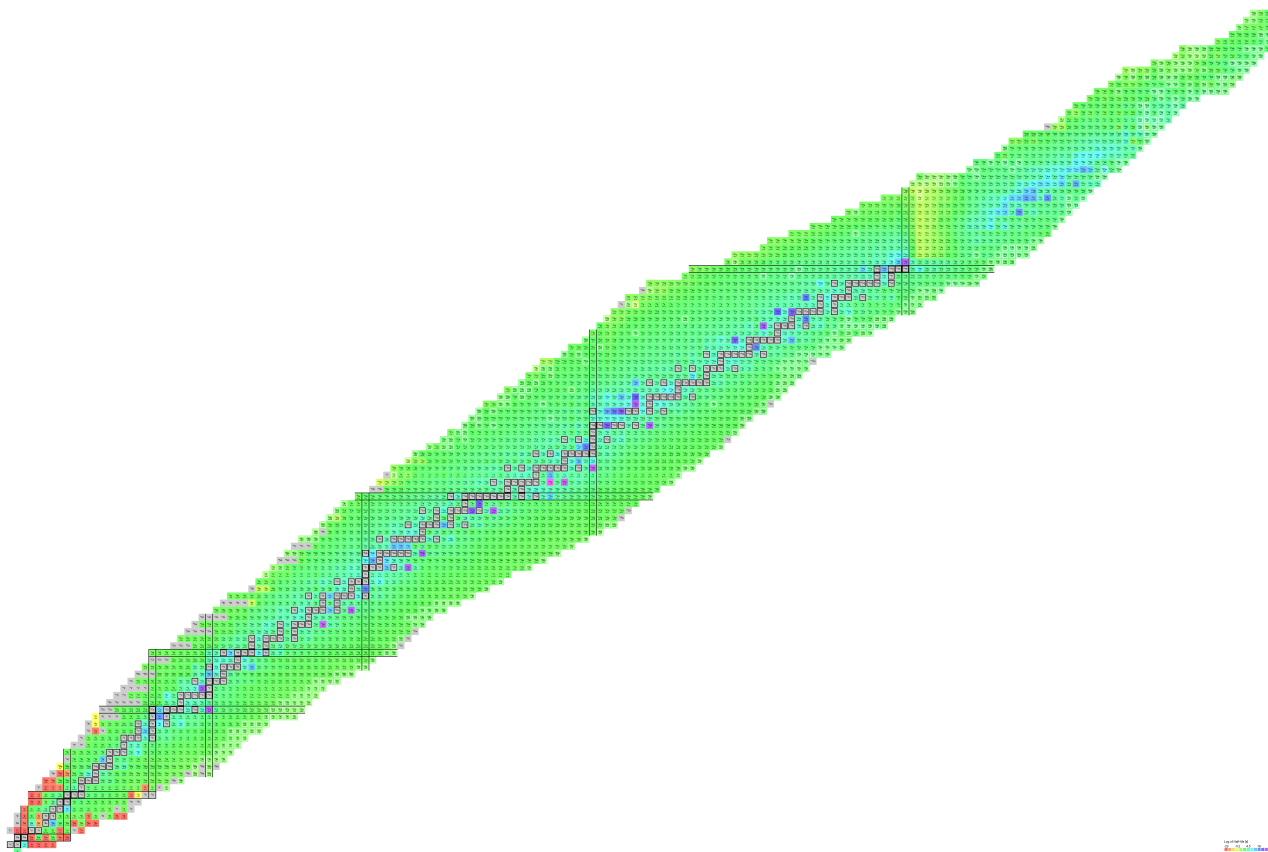
Fig. 3. *A nuclide chart plotting mass number (x-axis) against atomic number (y-axis). The colour shows the half life and runs from red to green to purple with increasing half-life. The black lines are the magic numbers. From Colourful Nuclide Chart[9]*
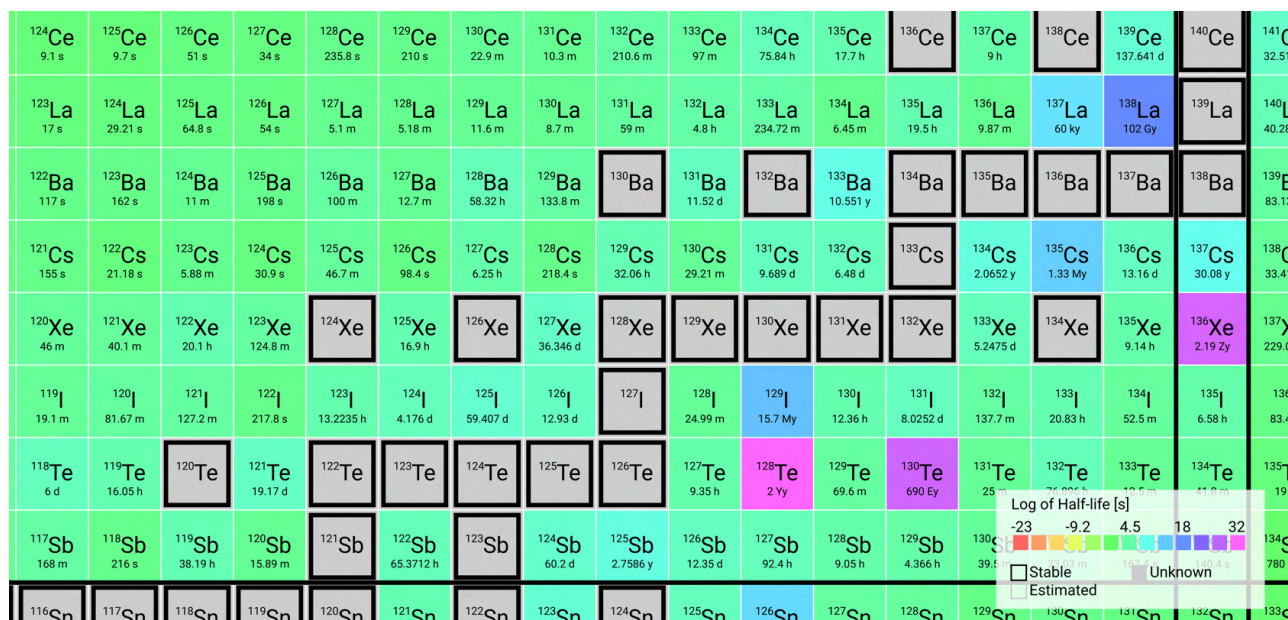
Fig. 4. *Nuclide chart focuses on the nuclei around xenon (x-axis increases by mass number, ,y-axis increases by atomic number). The stable isotopes are coloured gray with a black border. The unstable isotopes are coloured based on their half-lives. Note that ^{136}Xe is unstable but has half-life on order of 10^{21} years. Also note the ^{129}I that decays to ^{129}Xe with a half-life of 16My. From Colourful Nuclide Chart[9]*

adding a further neutron creates ^{122}Te through β decay of ^{122}Sb. From this, it can be seen that the run from ^{128}Xe to ^{132}Xe are the only Xe isotopes produced by the s-process.

Due to the s-process never straying far from the line of stability, all the intermediate nuclei are well studied and well understood. This means that the resultant nuclei can be accurately predicted[10].

2.1.2   R-process

The r-process occurs in environments with very high concentrations of energetic neutrons. These neutrons are captured by the nuclei faster than they can decay. This means that the nucleus will capture neutrons till any further neutrons can not be added faster than photo-disintegration, reaching an equilibrium. Then β decay occurs allowing the nucleus to reach a new equilibrium. Eventually, the high neutron flux stops and the neutron-capture/photo-disintegration equilibrium can no longer be maintained. Then β decay will happen till a stable isotope is reached.

On figure 4, the r-process will create strongly neutron heavy nuclei which can be seen along the bottom right edge (e.g. ^{132}Sn, ^{131}Sn). Once the neutron flux ends, these neutron rich nuclei β decay and move diagonally up and left. This means that all the Xe isotopes (with the exception of ^{124}Xe, ^{126}Xe, ^{128}Xe and ^{130}Xe) are produced. These Xe isotopes are shielded from the r-process by long lived isotopes (such as ^{128}Te and ^{130}Te) that exist in the way of the β decay path.

The details of the r-process depend on the properties of very unstable neutron rich nuclei. Due to their instability, they are not well studied. This means that the exact r-process cannot be accurately modelled and predicted.

2.1.3   P-process

Though the vast majority of heavy nucleons are produced by neutron addition processes (s- and r- processes) nuclear synthesis can occur through proton addition. This is called the p-process and results in proton heavy nucleons (as opposed to the neutron heavy nucleons favoured by the other two processes). In an analogous process to the s-process, the p-process works by adding a proton to the nucleon, which then undergoes β^+-decay[5]. This has the overall effect of first increasing both atomic weight and mass by one (the proton addition) then successively decreasing the atomic number by one (β^+-decay)

In contrast with the neutron addition processes, the p-process must overcome the Coulomb barrier. This makes it very rare. In xenon, the p-process only contributes to ^{124}Xe and ^{126}Xe which form a negligible amount of the overall composition. Thus, they are neglected in this report.

---

[5]This differs from the more common β^--decay by instead changing one proton to a neutron and releasing a positron

2.1.4 Abundances of neutron capture elements

In a way analogous to electron shells, there are some nuclei numbers that are especially stable. This happens due to the nucleons arranging themselves into shells within the nucleus. These magic numbers are: 2, 8, 20, 28, 50, 82 and 126. This means that nuclei with proton number or neutron number equal to a magic number are especially stable. This is even more so for doubly magic nuclei where both the neutron number and proton number are equal to a magic number.

The r- and s- processes both pile along magic numbers. The s-process piles up because the neutron capture cross-sections are smaller for magic numbers. The r-process piles up for a different reason. As the nuclei capture neutrons during time of high neutron flux, their path through the nuclide chart kinks upward due to β decay. At magic numbers, the β decay rate tends to be slower than their neighbours'. This means that the nucleus undergoing r-process spends longer as a magic number nucleon.

For the s-process nuclei, this means that magic number nuclei that lie on the s-process path are produced in excess. The r-process will pile up at neutron heavy magic number nuclei and β decay from there.

This has a visible effect on the relative abundances of nuclei, as can be seen in figure 5. Of note in figure 5 are the sharp s-process peaks at the magic numbers (^{88}Sr, ^{138}Ba, ^{208}Pb) and the broad r-process peaks that come just before the magic numbers (Ge, Xe, Pt)

2.1.5 Stellar sources

As low and mid mass stars near the end of their life, they run out of hydrogen in the core. They then leave the main sequence (the line from bottom right to top left in figure 1) and switch to burning hydrogen in a shell (Red Giant Branch see fig 6a). Very low mass stars cannot start the helium fusion for further nuclear reactions so will cool down to a white dwarf. Larger stars ($> 2M_\odot$) initiate helium fusion and contract before re-expanding. These stars are now in the Asymptotic Giant Branch (AGB, see fig 6b). Stars much larger than the sun will eventually burn carbon, oxygen and heavier elements. As these stars age, the burning of heavier and heavier elements occurs in the core. In addition, fusion of lighter elements occurs in the shell. Together, this means that there is a large amount of convection which brings significant amounts core material to the surface. This material is ejected through star's stellar wind.

As the core changes what it burns, large shock waves of collapse and expansion move though the star and eject the outer shell (which has by now been enriched by core material). Due to this, AGB stars are the main source of the s-process material in the interstellar matter.

High mass stars instead form red supergiants. As they age, they too leave the H-burning main sequence and switch to burning heavier and heavier elements and produce an enriched wind. How-
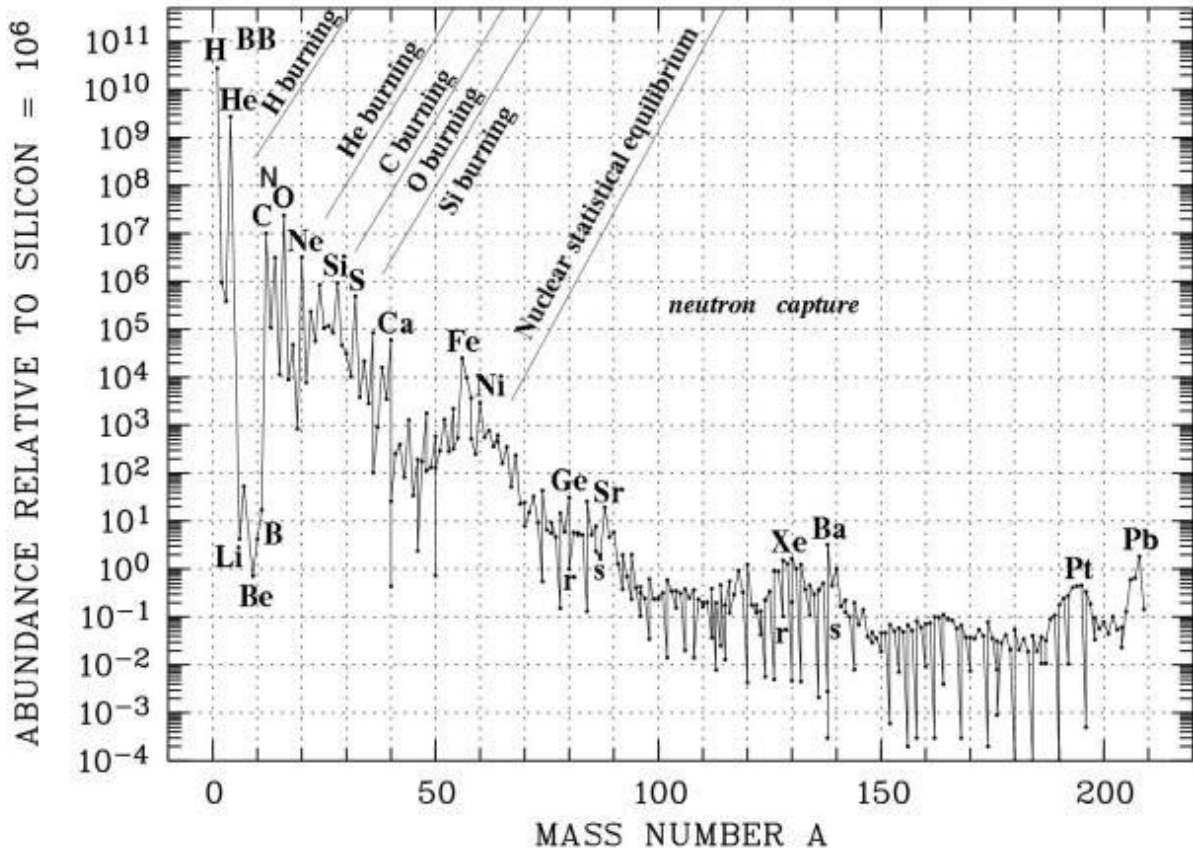
Fig. 5. The relative abundances of nuclei. Note that the magic numbers are: 2, 8, 20, 28, 50, 82 and 126. The s-process peaks are at: ^{88}Sr (50 neutrons), ^{138}Ba (82 neutrons), ^{208}Pb (82 protons, 126 neutrons). The r-process peaks are slightly lighter at: Ge, Xe, Pt
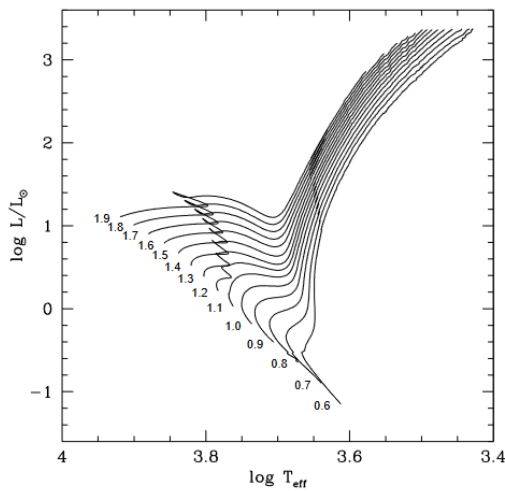
(a) Evolution of low mass stars ($0.6 M_\odot$ to $1.9 M_\odot$)
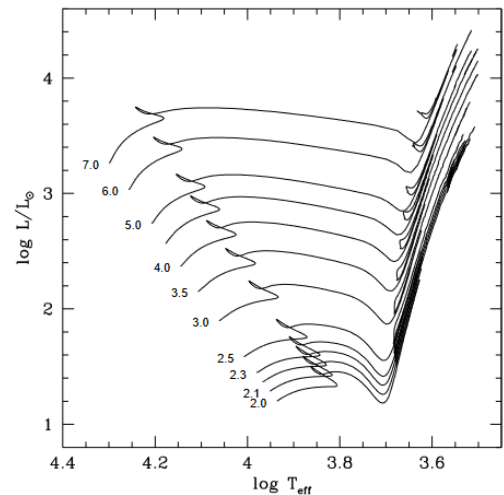
(b) Evolution of mid mass stars ($2.0 M_\odot$ to $7.0 M_\odot$)

Fig. 6. This figure shows the evolution of low (fig 6a) and mid (fig 6b) mass stars. Figure from Girardi et al. [11]. These plots have the Luminosity on vertical axis and temperature of emitted light on the horizontal axis. The main sequence is outlined by the starting points of the tracks. The low mass stars leave the main sequence and join the Red Giant Branch (RGB). The mid mass stars take a different path. They leave the main sequence, join the RGB and then leave the RGB (see the kink in fig 6b where the tracks temporarily reverse directions). They then start behaving again like red giant stars. This is known as the Asymptotic Giant Branch (AGB)
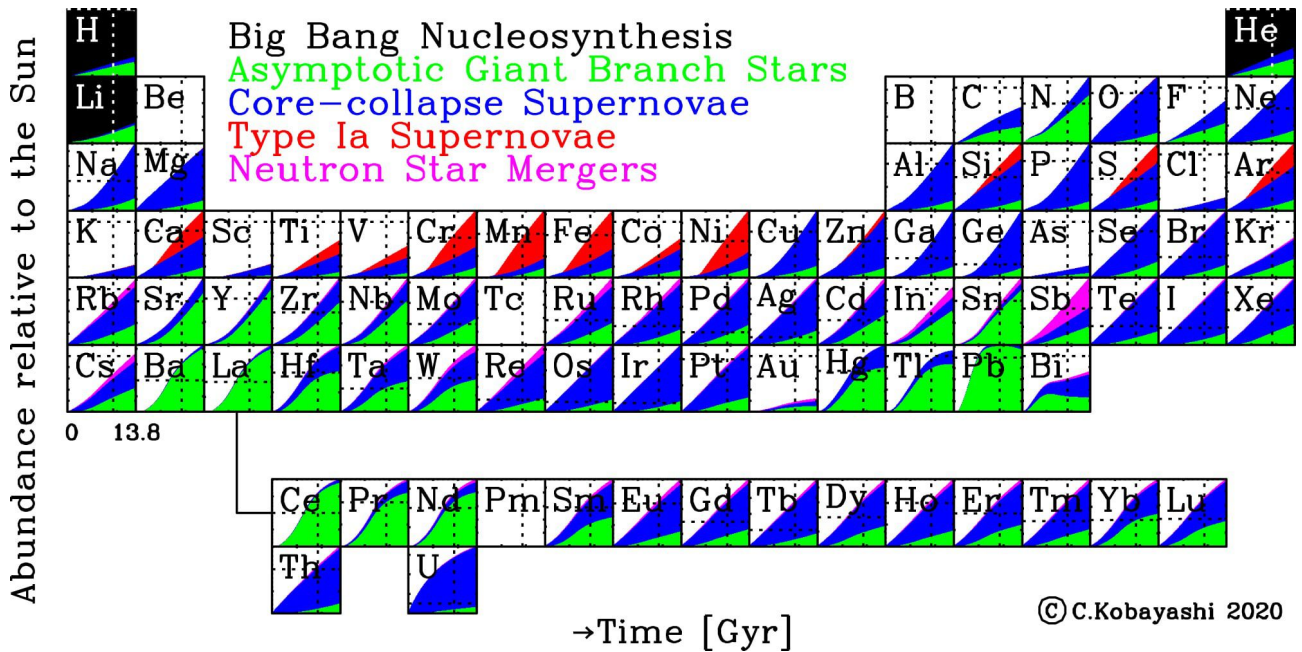
Fig. 7. *Periodic table showing the origin of each element within the Galaxy as well as the abundance relative to the Solar System. The solar abundances are shown in the dotted lines within each square. Note that amounts returned by stellar mass loss are also included for AGB stars and core-collapse supernovae.[17]*

ever, a higher proportion of their mass is ejected into the ISM when they die through supernovae. This occurs when the core reaches the stage of producing iron which can no longer be used to generate more energy. Instead, the core eventually produces iron which has the highest binding energy per nucleon, meaning any further rearrangement of these nucleons is endothermic in energy and no longer releases useful energy. This means that the iron accumulates in the core until it grows to such a size that it can no longer support itself through electron degeneracy. This collapsing core eventually goes on to form a neutron star or a black hole. This collapse generates large amounts of neutrons which causes the outer layers to be ejected and produces r-process elements within them.

Newer research has suggested a new source for r-process elements, namely neutron star mergers[12][13][14][15][16]. This happens in a system with one or more neutron stars. As they orbit each other, they loose energy and eventually collide. This releases large amounts of neutron into the surrounding area. These neutrons then cause nucleosynthesis to occur through the r-process.

2.2 Xenon

This paper will focus specifically on xenon. Xenon lies within an r-process peak (fig. 5) and has many stable isotopes[6]. The distribution of isotopes can provide a map of the r-process. In addition, the s-process also contributes to xenon.

---

[6] 9 stable isotopes, although ^{136}Xe is technically unstable but has a half life on the order of 2.18×10^{21} yr

Table 1. *Genesis measurement of Xe in the solar wind [18]. All numbers are relative to ^{132}Xe.*

Isotope	rel. abundance	Process
136	0.3001 ± 0.0006	r
134	0.3691 ± 0.0007	r
132	1.0	s, r
131	0.8256 ± 0.0012	s, r
130	0.1650 ± 0.0004	s
129	1.0405 ± 0.0010	s, ^{129}I decay
128	0.0842 ± 0.0003	s
126	0.00416 ± 0.00009	p
124	0.00491 ± 0.00007	p
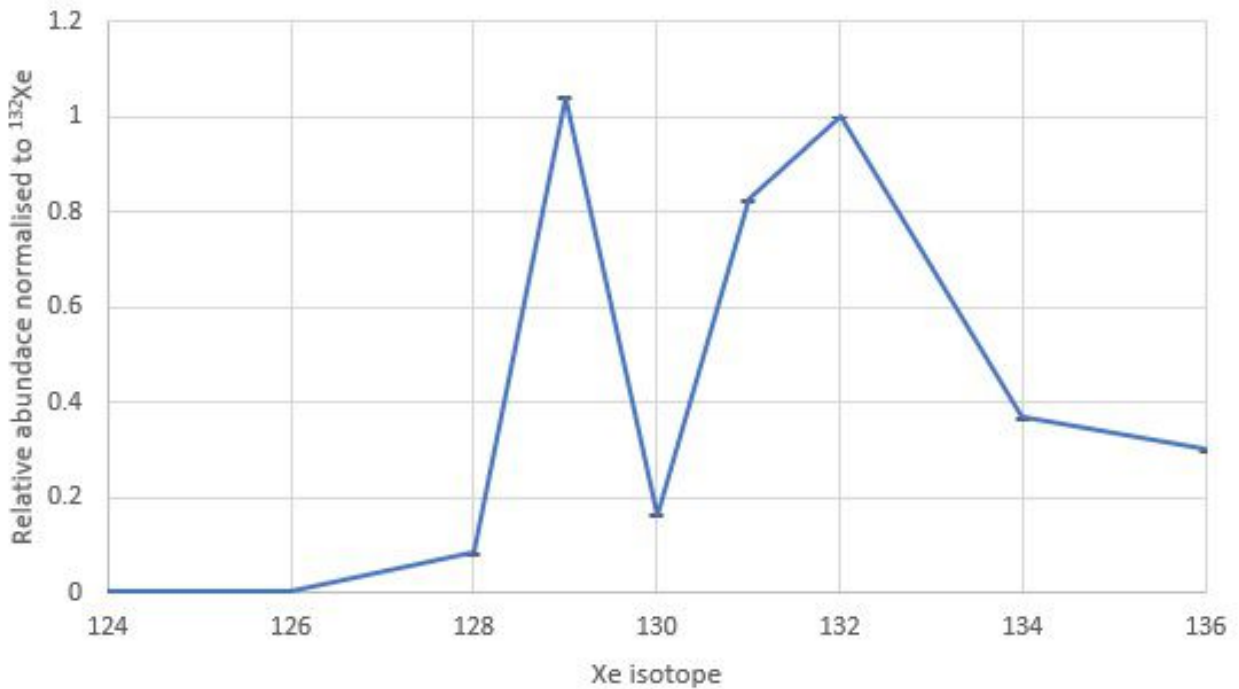
Fig. 8. *The relative abundances of Xe in the solar wind. Normalised to ^{132}Xe.[18]*

Our best knowledge of isotopic ratios of of the average Solar System material has been obtained by measuring the Xe composition within the solar wind. This was done by the GENESIS mission[18]. It spent two years collecting solar wind samples between 2001-2004 before returning the sample to Earth for analysis. The mission is best remembered for its unplanned hard landing. Despite this, the samples were safely retrieved and fully analysed.

The results are listed in table 1 and plotted in Fig. 8.

Of the 9 stable xenon isotopes, 2 are exclusively made by the r-process (^{136}Xe, ^{134}Xe); 1 exclusively by the s-process (^{130}Xe); and 2 exclusively by the p-process (^{126}Xe, ^{124}Xe). Also of note is ^{129}Xe which is made by the s-process but has significant contamination from the decay of ^{129}I and ^{128}Xe which is mainly made by the s-process but has contributions from the p-process. The remaining isotopes (^{132}Xe, ^{131}Xe) are made from a mixture of the s- and r-processes.

The p-process involves the capture of protons. However, this requires overcoming the Coulomb

barrier. Therefore, it only contributes trace amounts of ^{126}Xe and ^{124}Xe.

The r-process (which works by adding a large number of neutrons to a nuclide and then letting it β-decay) has very highly neutron rich intermediates. Most of these intermediates are very short-lived. However, occasionally, some of these intermediates are long-lived enough that they can cause variations in the final xenon populations.

Of note is ^{129}I, which decays through the β-process to ^{129}Xe. The different chemistry of iodine mean that it get separated from the main xenon population. In addition to this, ^{129}I is, itself, a decay product of heavier nuclides (such as ^{244}Pu with a half-life of 80 Myr). This means that further ^{129}I is produced much till long after the formation of the Solar System.

Xenon, like other noble gases, is very unreactive and extremely volatile. Therefore, it is mainly present as a gas in the ISM. A small fraction can be implanted or adsorbed within crystal grains in space. This can happen in the ISM, but also in the original stellar winds. There are occasional presolar grains have that acquired noble gases through implantation by existing close to their parent star. These presolar grains preserve the isotope mix of the parent star. The Sun formed from the ISM, which has a gas to dust ratio of at least 150:1 [19] so it does not contain a significant contribution from these presolar grains.

2.2.1 Xenon in the Solar System

The Sun formed from a collapsing interstellar cloud. As the moment of inertia of the cloud decreased, its angular momentum caused the particles to orbit around the proto-Sun in a disk. The planets and other solid bodies formed within this disk.

When fusion started within the Sun, the resultant solar wind drove out the gas phase. This reduced the disk to solid grains only. Jupiter and Saturn formed before this happened, and they kept gases such as hydrogen and helium, objects that formed later consists only of the solid particles. For object within the snow line, this includes silicon and iron. The objects further out from the snow line, which is within the asteroid belt, also formed from significant amounts of solid H_2O and CO_2, the so-called ices.

The inner rocky planets are primarily composed of silicon, iron and other refractory elements. Jupiter and Saturn are the gas giants and are primarily composed of hydrogen and helium. Ice giants like Uranus and Neptune are primarily composed of ices like H_2O, CO_2 and CH_4. Asteroids form at the border of the snowline. Therefore they form as a mixture of rocky and icy bodies. Comets originate from the Kuiper Belt and the Oort Cloud which are well beyond the snow line and are therefore almost entirely composed of ices.

In the interstellar matter, xenon is primarily in the gas phase. When the Sun formed, all the xenon was driven off with only the xenon that was adsorbed onto other grains surviving in the inner So-

lar System. Beyond the snowline, however, the xenon can survive in the gas phase. This means that the xenon found in the inner planets like Earth are a mix of the xenon originally from the inner Solar System (that was preserved in grains) and the xenon introduced by the outer Solar System (introduced by comets hitting these planets).

The Earth atmosphere has two main sources: outgassing from volcanic events and input from cometary bombardment. The outgassing will have the same xenon composition as the material that formed the original Earth plus any products from nuclear decay. The comets will provide material that formed in the outer Solar System.

The formation of the rocky planets started with grain-grain collisions. Over time, this caused these grains to grow and become large enough for gravity to play a deciding factor. Some of these grains include Calcium-Aluminium Inclusions (CAIs) which are some of the oldest material found within the Solar System.

2.2.2 Compositional variation across the Solar System

There are several isotopes that show significant variation across the Solar System. This is especially apparent in short lived nuclei such as ^{54}Cr[5] and ^{26}Al[6]. Xenon also shows significant variation amongst its isotopes. This heterogeneity could have been created through internal processes within the Solar System. This could include chemical reactions or mass fractionation. The other possibility is that this variation was caused by some external cause such as a late injection of some material into the Solar System or the ISM that went onto form the Solar System started out poorly mixed.

This internal processes cannot explain xenon's isotopic variation. This is because xenon is a noble gas and, thus, unreactive. This means that chemical reactions including xenon do not occur at the low temperatures required for there to be measurable differences between isotopes. Mass fractionation has a low effect as xenon has a very high atomic mass and thus very little relative difference in mass between the heaviest and lightest isotopes. This means that the effect of mass fractionation is minimised. Thus significant variation between xenon compositions require an explanation that is external to the Solar System.

This leaves two possible explanations: either the heterogeneity was present before the Solar System formed or the heterogeneity was formed by an injection of matter into the Solar System as it was being formed. In the case that the heterogeneity was present in the ISM prior to the formation of the Solar System, this heterogeneity has to be maintained throughout the formation of the Solar System. A possibility for this could be that the different types of material phases (gaseous phase material, icy grains, refractory grains) trap different compositions of xenon. This will lead to heterogeneity in the modern Solar System as only the refractory grains will survive in the inner Solar System, while the icy material will survive in the outer material (beyond the asteroid belt) while
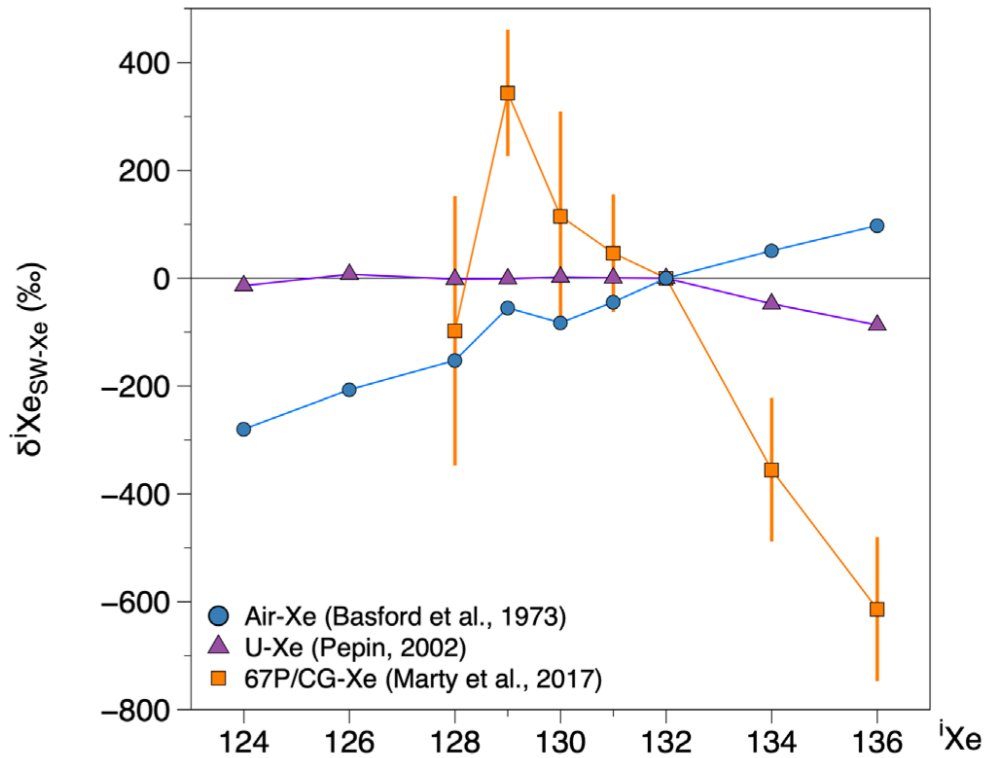
Fig. 9. *Some common compositions that have been normalised to the isotope composition in the solar wind [20]*

Table 2. *This table contains a summary of various xeonn compositions found throughout the compositions. Some of these compositions (such as Xe-SW, Xe-Air, Xe-Q) are measured directly from a source, while others (such as Xe-U, Xe-s) are calculated based on other factors.*

Composition	Notes
Xe-SW	Measured in Solar wind
Xe-Air	Measured in Earth atmosphere
Xe-U	Calculated original composition of the Earth
Xe-Q	Measured in meteorites
Xe-67P/CG	Measured in comet 67P/Churymov-Gerasimenko
Xe-s	Calculated contribution by the s-process
Xe-r	Calculated contribution by the r-process

the gaseous phase only survived in Jupiter and Saturn which had gravity wells strong enough to overcome the solar wind when fusion burning started in the Sun. A late addition of material will preferentially distribute material to the outer Solar System. Exchange of material between inner and outer Solar System slowed down significantly after the formation of the gas giants. This will maintain this heterogeneity to the modern day.

Xenon has significant variation in its isotopic composition across the Solar System. For ease of reference, the isotope compositions found in different places (namely: in Earth atmosphere, in solar wind, in asteroids, in comets) differ and each composition is given their own name. Some relevant compositions are: Xe-Air, Xe-U, Xe-SW, Xe-Q, Xe-s. A summary can be seen in table 2

Xe-SW is the xenon composition found in the solar wind. This was measured by the Genesis mis-

sion[21][18]. It is considered to be the bulk composition of the Solar System, due to the Sun comprising of over 99.9% of the Solar System mass and is the composition against which the other compositions are generally compared.

The xenon composition found in the current atmosphere of Earth is called Xe-Air. It is enriched in fission products. The largest addition from fission is due to β-decay of ^{129}I (which has a half-life of 15.7 Myr) to ^{129}Xe. In addition to this, it has undergone mass fractionation compared to Xe-SW. By accounting for and removing the effect of ^{129}I and other fission products, and then the mass fractionation on Xe-Air, the original Xe composition of Earth can be inferred. This composition is called Xe-U[7]. Compared to Xe-SW, Xe-U has too little of ^{134}Xe and ^{136}Xe(depleted by 5% and 9% respectively relative to Xe-SW[20]).

Xenon is found within CAIs within chondritic meteorites. Since these grains date to before the formation of the Solar System, they can be used to probe those conditions. The composition found there is called Xe-Q[8].

Similarly to meteorites, comets also preserve grains dating to before the formation of the Solar System. However, very few comets have been measured. The STARDUST mission collected dust samples from the coma of Wild 2. However, the ROSETTA mission is the only mission which has so far returned samples from the surface of a comet (67P/Churyumov–Gerasimenko in this case). Xe-67P/CG has a significantly different composition to other compositions. It is especially deficient in the heaviest isotopes. Marty et al. [8] found that Xe-U can be produced by mixing Xe-67P/CG with Xe-SW, with the final Xe-Air composition being $22 \pm 5\%$ Xe-67P/CG.

2.2.3   Inferring the r-process composition

As mentioned in section 2.1.1, The s-process is well modelled and well understood, while the r-process is less so. Xenon has significant contributions from both the r- and s-processes. The isotopic distribution resulting from the s-process (Xe-s) can be calculated. This has been verified by checking against the compositions in SiC grains[22]. By subtracting a scaled s-process composition, the bulk r-process abundances can be inferred. As can be seen in table 1, ^{130}Xe is produced only by the s-process. Therefore, by scaling the s-process composition (calculated by Lewis et al.[23]) to match the ^{130}Xe, all the s-process contribution can be removed.

By thus subtracting Xe-s from various xenon compositions found across the Solar System, different estimations for Xe-r (the xenon composition produced by the r-process) can be produced. By comparing the ^{134}Xe/^{132}Xe against ^{136}Xe/^{132}Xe ratios of the resultant r-process estimates can be seen (as seen in fig. 10). Since the variation lies on a straight line, this suggests that the variation present among the compositions is due mixing between two populations. This was the conclusion reached by Gilmour and Turner[24].

---

[7]U for ur
[8]Q for quintessential
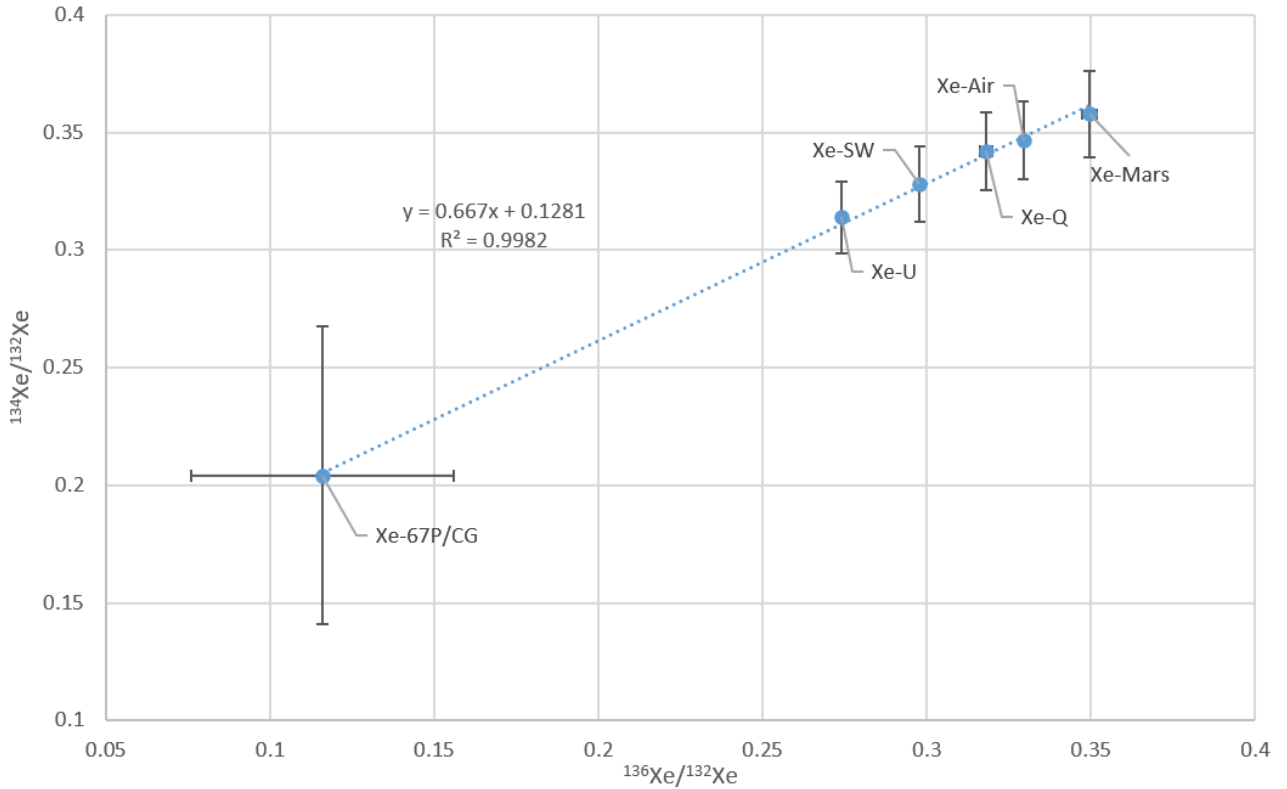
Fig. 10. *Variance between $^{134}Xe/^{132}Xe$ against $^{136}Xe/^{132}Xe$ ratios in the various xenon compositions once Xe-s is removed. Note how this variation lies on a straight line, suggesting that the ^{136}Xe, ^{134}Xe and ^{132}Xe variation occur because of mixing between two populations. Note that there are much larger error bars on the comet data, In addition the errors for the $^{136}Xe/^{132}Xe$ ratios are smaller than the symbols for the non-comet compositions.*

This implies that there are multiple r-process sources to explain the the two r-process composi-tions. Because each of the measured compositions come from large reservoirs, this also implies that a large amount of matter has been contributed from each of these processes. This was ex-plored by Wasserburg et al. [25] where the r-processes differ due to neutron density. Research exploring the ejecta of neutron star mergers (NSM) suggest a possible site for a different r-process to occur. Following the detection of a γ-ray burst associated with a neutron star merger[13], there was now evidence that NSM have the r-process occur within them[12]. Hotokezaka et al. [14] com-piled much of the evidence of the previous decade and ran simulations to conclude that NS merg-ers provide significant amount of r-process matter.

As mentioned above, the xenon isotopic ratios in the Solar System can be understood as a mixing between two components with different isotopic ratios. This can be explained if there are two dif-ferent r-processes in existence which give different isotopic ratios. One of these may be the neu-tron star mergers, and the other one can arise from traditional (core-collapse) supernovae.

Supernovae are common. In the Milky Way, we would expect a core collapse supernova to happen once every 61^{+24}_{-14}yr[26]. Neutron star mergers are far less common. The rate has been measured from gravitational wave detections. Scaling from the rate in the local Universe (48Gpc^{-3}yr^{-1}), the rate for the Milky Way is estimated as 21^{+28}_{-14} Myr^{-1}[27].

Based on these different rates of occurrences, we can conclude that the supernovae will create a baseline enrichment throughout the Milky Way. The much rarer neutron star mergers will provide stochastic enrichment.

2.2.4   Change in Xe composition in Solar System

As the ^{134}Xe/^{132}Xe ratio against ^{136}Xe/^{132}Xe ratio in the measured xenon compositions lie along a straight line (see Fig 10), the presence of two end members can be inferred. By considering the amount of ^{136}Xe, a low ^{136}Xe member must have a ^{134}Xe/^{132}Xe ratio less than 0.12 while the high ^{136}Xe member have ^{134}Xe/^{132}Xe be greater than 0.35.

This can be modelled by considering an initial solar composition (Xe-SW) and a hypothetical low ^{136}Xe member. These two compositions add together to form the cometary composition, as seen in equation 1. Here, C, S and A are the cometary, solar and injected compositions. a is the proportional contribution of A to C and is calculated in equation 2.

$$C = aA + (1 - a)S \tag{1}$$

$$a = \frac{S - C}{S - A} \tag{2}$$

By using the ^{136}Xe/^{132}Xe values, we get $C = 0.12 \pm 0.04$ and $S = 0.298 \pm 0.001$. The value for A can only be limited to be smaller than C. To minimise a, $A = 0$ is chosen. This gives the result of $a = 0.61$. By using the 2σ errors for the C and S, a lower limit of $a > 0.34$ can be found with 97.5% confidence.

Equation 1 assumes that the cometary composition was formed after Xe-SW, the solar composition. This is discussed further in section 5.

This value of $a = 0.34$ is used for the model. The aim of the model is to identify what fraction of the ISM could be destined to form a system like the Solar System which would experience an increase of 34% or more in its contribution from neutron star mergers on a timescale consistent with the formation of comets after the composition of the parent star is set.

Note that this analysis assumes that the reason for the xenon composition to differ between comets and the solar wind is because the comets have included matter from a source that is not present (or much less present, proportionally) in the Sun. Specifically, while the Solar System is forming, some injection of matter causes the outer parts of the Solar System to change its resultant xenon composition. This injection will have a much less significant effect on the Solar composition as much of the Sun's matter will have already condensed onto itself by this point and the injected matter is insignificant compared to the mass of the Sun.

3 Methods

3.1 Model parameters

The Milky Way is modelled as a two dimensional plane made up of pixels. A neutron star merger goes off in a randomly chosen pixel. The ejecta from the NSM are then evenly distributed to all pixels within a threshold distance and added to the material already there. In subsequent time-steps the ejecta are diffused to nearby pixels in a similar way. In addition, during each time step, the Galaxy is rotated using a rotation curve as model parameter. The rotation changes which pixels are adjacent to each other and has the effect of speeding up overall diffusion. The amount of ejecta neutron star mergers is tracked for each pixel at each time step.

3.1.1 Timestep

The rate of neutron star mergers in the Milky Way is 24.1 Myr^{-1}[27] whilst the rate of supernova events is 0.0163 ± 0.46yr^{-1}[26]. Even if only $\sim 1\%$ are major sources of r-process elements[28], by comparing these rates it can be seen that neutron star mergers are comparatively rare events. This allows the supernovae ejecta to be modelled as a constant background and neutron star mergers as stochastic events.

The Milky Way is roughly 13.4 Gyr old while the Solar System formed roughly 4 Gyr ago. Meaning 10 Gyr must be simulated.

The main limiting factor is the time taken to run the simulation. It was decided to use a timestep of 50 Myr.

3.1.2 Rotation curve

Reid et al.[29] used measurements of proper motions of masers closely associated with stars to give the rotation curve of the Milky Way. They found that between the radii of 5-16 kpc, the rotation curve is nearly flat with a slope of -0.2 ± 0.4 kms^{-1}kpc^{-1}. They also found that the Sun has a circular rotational speed of 240 ± 8 kms^{-1}.

$$\theta(R) = \begin{cases} 0.00102 \times 48T, & \text{for } R < 5 \\ 0.00102 \times \frac{240}{R}T, & \text{for } R > 5 \end{cases} \tag{3}$$

In the model used for this paper, equation 3 was used to simulate the rotation θ (in radians) of a point at radius R (in kpc) over timestep T (in Myr). This is a flat rotation curve of 240 kms^{-1}kpc^{-1} at

radii larger than 5 kpc. At smaller radii, a straight line is used from $0\,\mathrm{kms^{-1}kpc^{-1}}$ to $240\,\mathrm{kms^{-1}kpc^{-1}}$. The multiplier, $0.001\,02$, converts this angular velocity from $\mathrm{kms^{-1}kpc^{-1}}$ to $\mathrm{Myr^{-1}}$. This also means that the model will only produce relevant data between 5-16 kpc.

3.1.3   Diffusion constant

A simplified diffusion model is used to run the simulation. The following loop runs for every pixel in the Galaxy.

1. The current pixel will be considered the source of diffusion for this step.

2. A threshold distance is calculated using equation 4

3. The pixels that are within this distance to the pixel currently being considered are noted

4. A value of P/n is added to these nearby pixels. P is the amount of matter within the pixel being considered. n is the number of nearby pixels

5. The amount of matter in the current pixel will be changed from P to P/n as the matter that was originally here has now been distributed

Within this model, diffusion is done by distributing the matter within a pixel evenly among all pixels within a diffusion distance, d. Beniami and Hotokezada[30] give a diffusion constant of $c <$ $0.1\,\mathrm{kpc^2Gyr^{-1}}$ for turbulent gas diffusion on the observed r-process abundances in MW stars. From this, equation 4 is used to calculate the diffusion distance d (in kpc), using timestep T (in Myr). Based on the chosen timestep of 50 Myr, this gives a value of 0.071 kpc to d.

$$d = \sqrt{(cT/1000)} \qquad (4)$$

3.1.4   Pixel size

The inner and outer radius limits for which the rotation curve (eq. 3) is valid are 5 kpc and 16 kpc. To remove the edge effects, the model will run from the full range from 1 kpc to 20 kpc, while only analysing the data from 5 kpc to 15 kpc. This way all edge effect are removed.

The angular distance between pixels is chosen so that the distance between adjacent pixels with the same radius is same as the distance between radii. This can be seen in figure 11, where a distance of 0.5 kpc is chosen for visibility.

The diffusion distance, d, as given by equation 4, imposes an upper limit to the pixel size. However, the pixel size cannot be too much smaller, for the number of pixels grows very quickly (as can
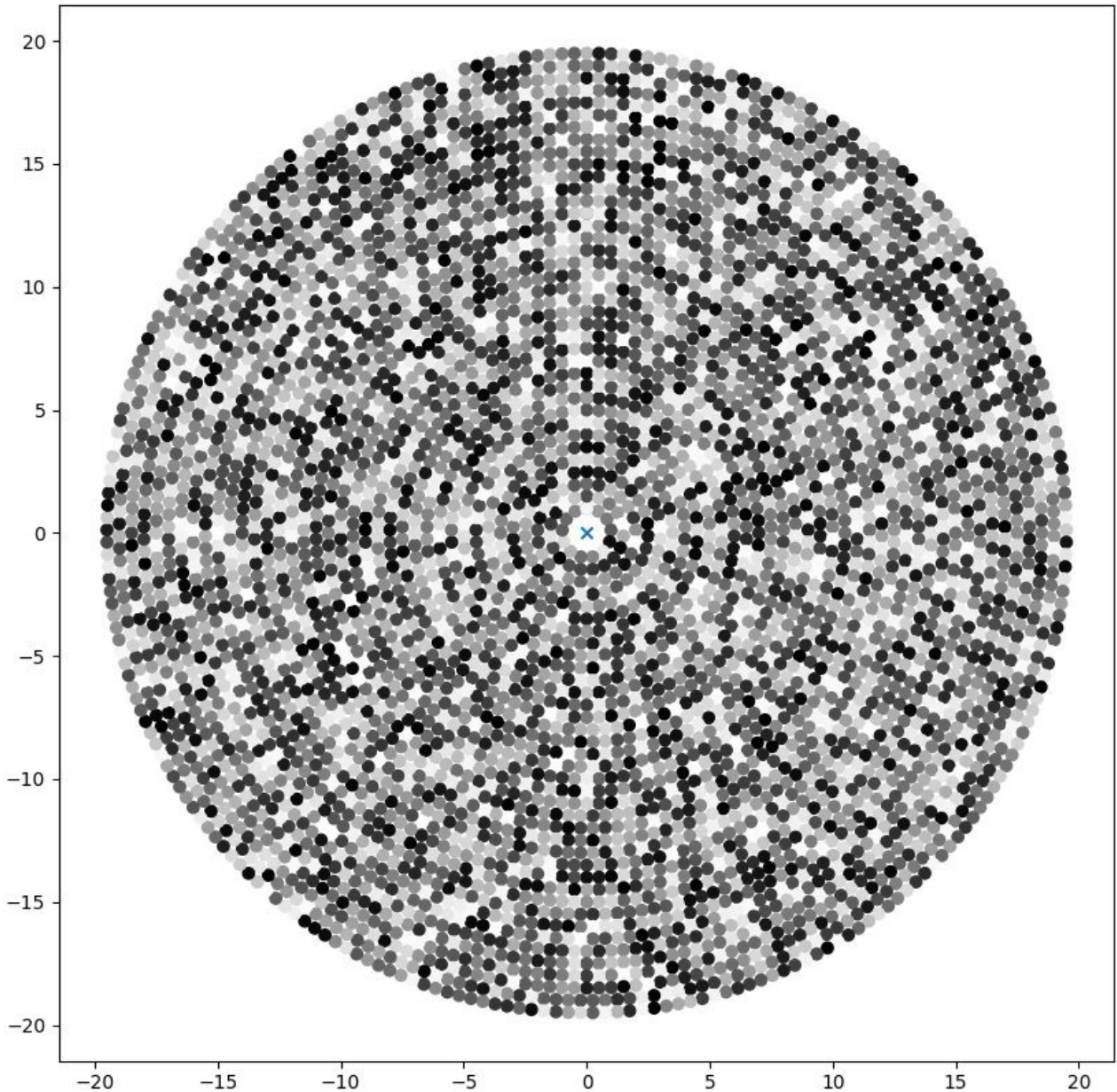
Fig. 11. *This shows how the pixels are distributed throughout the Galaxy. Note how the distance between pixels is the same whether the pixels are at the same radius or in adjacent radii. In this case, the distance between adjacent pixels is* 0.5 kpc *and the inner and outer limits are* 1 kpc *and* 20 kpc.

be seen in figure 12). This can slow the simulation significantly. Based on the chosen timestep of 50 Myr and the resulting diffusion distance of 0.071 kpc, a pixel size of 0.06 kpc was chosen.

3.1.5   Rate of neutron star mergers

Chruslinska[27] gives a rate of neutron star mergers of 24.1 Myr^{-1}. Therefore, during each individual timestep of 50 Myr, there are 1,205 merger events. These are distributed evenly across the Galaxy. Though stars are only formed within the star forming regions, NSMs do not correspond to these areas. This is because of the very large delay between the birth of a star and that star becom-
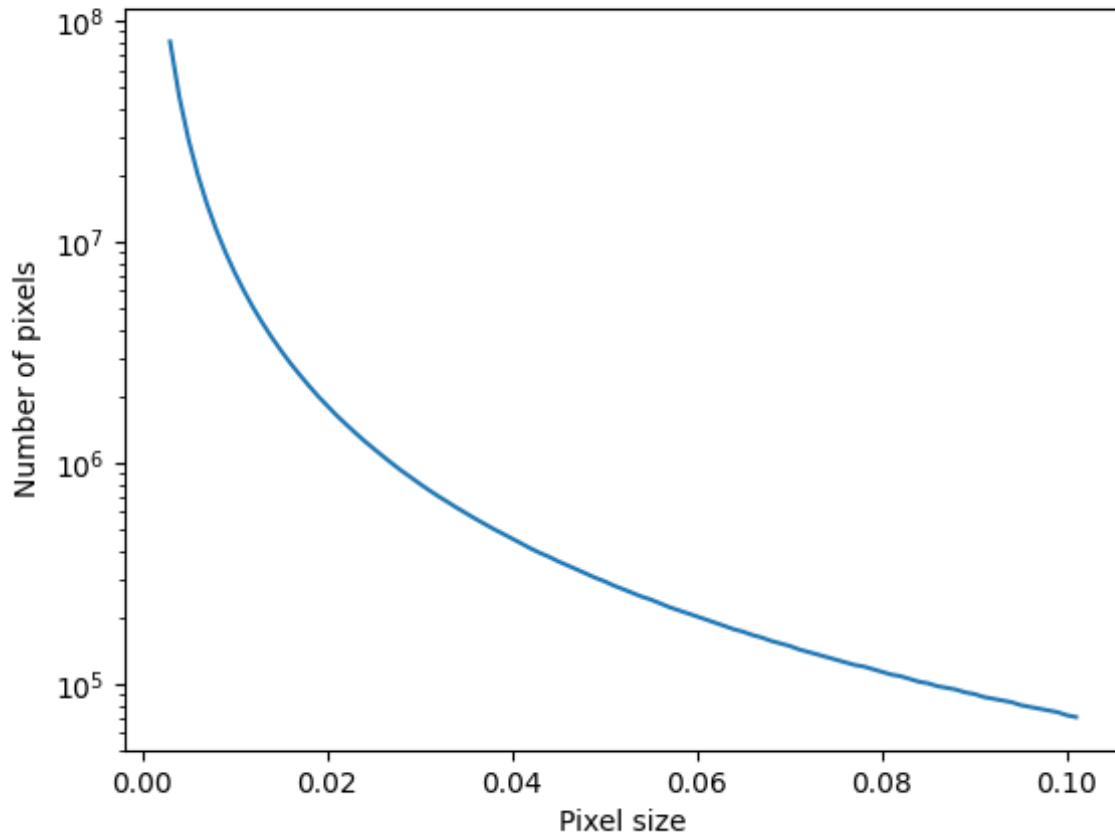
Fig. 12. *This shows how the number of pixels in the model grows very fast as the distance between radii decrease.*

ing involved in a NSM. In this analysis, it is assumed that these neutron star mergers are distributed evenly across the galaxy.

3.1.6 Fractional change

From figure 10 the minimum amount of injected mass can be estimated. First, a hypothetical injected composition with no ^{136}Xe is theorised. This is done because such a composition will give the maximum change per added mass, thus it will give an estimate for the minimum required amount of added mass. Then it is assumed that this composition is the cause for all the difference between Xe-SW and Xe-67P/CG.

The relevant values are: the ^{136}Xe/^{132}Xe ratio of the bulk Solar System (this is taken to be Xe-SW, 0.2978 ± 0.0012) and the ^{136}Xe/^{132}Xe ratio of the outer Solar System (taken to the Xe-67P/CG 0.12 ± 0.04). By using the 2σ errors, a minimum fraction of matter added by injection of 34% is calculated.

The model gives an amount of NSM ejecta in each position in pixel. By using equation 1 and setting $A = 0$, a can be calculated using equation 5. Here C and S are the cometary and solar composi-

Table 3. *This table lists the different parameters used for the various models. Note that model 2 is considered the full model upon which the analysis is conducted. Models 1a and 1b are demonstration model to show the effect of galactic rotation on diffusion of matter.*

Model	Parameters
1a	Timestep: 50 Myr Threshold diffusion distance: 0.707 kpc NSM rate: *only single event modelled*
1b	Timestep: 50 Myr Threshold diffusion distance: 0.223 kpc NSM rate: *only single event modelled*
2	Timestep: 50 Myr Threshold diffusion distance: 0.071 kpc NSM rate: 24.1 Myr^{-1}

tions.

$$a = \frac{S - C}{S} = \frac{P_t - P_{t+s}}{P_t} \tag{5}$$

Using equation 5, the model can also be linked to a. Here, P_t is the composition in a pixel before the time of formation of the Solar System and P_{t+s} is the composition in that same pixel after the time of formation of the Solar System. Therefore, calculating a fractional change over time within pixel the heterogeneity within the Solar System can be approximated.

4 Results and discussion

4.1 Model method

The model works by stochastically adding r-process material throughout the Galaxy. This matter is then diffused through the Galaxy while the effect rotation is taken into account. This matter is tracked by dividing the galactic plane into pixels. These pixels are arranged in rings and the separation of pixels within a ring is set to be equal to the separation between rings.

The colour of the pixel indicates the amount of ejecta from the neutron star merger. Specifically the amount of ^{136}Xe that is ejected from this r-process. Within the figures, the pixels with the most matter is coloured black and the least white.

In addition to this, the rotation that occured between timesteps is corrected for. This way, the Galaxy can be compared at different times without losing track of pixels.

4.1.1 Single event

Figures 14 and 13 shows the diffusion of a single NSM event. This uses the same rotation curve described in equation 3. However, it uses a bigger diffusion constant (10 kpc^{2}Myr^{-1} for figure 13 and 1 kpc^{2}Myr^{-1} for figure 14) than the actual. This is so as to clearly show the diffusion pattern.

To match the conditions for the Milky Way, the following parameters must be matched:

- Rotation curve:

    - 240 kms^{-1} between 5 kpc and 15 kpc

    - linearly increasing to 240 kms^{-1} for under 5 kpc

- Diffusion constant:

    - 0.1 kpc^{2}Gyr^{-1}

- Neutron star merger rate:

    - 24.1 Myr^{-1}

Rotation curve is a flat line at 240 kms^{-1} between the radii of 5 kpc to 15 kpc. This is based on the work by Reid et al.[29]. Diffusion occurs by distributing the matter within a threshold distance determined by $\sqrt{Tc}$, where T is the timestep and c is a diffusion rate, determined by Beniamini and Hotokezada[30] to be 0.1 kpc^{2}Gyr^{-1}. However, for this toy model (model 1b in table 3), a larger diffusion rate of 10 kpc^{2}Gyr^{-1} was used. The Galaxy is simulated from 1 kpc to 20 kpc, however only the range from 5 kpc to 15 kpc is used for analysing. This is because this is the region determined by Reid et al.[29] to have a roughly flat rotation curve. This region also includes the Solar System which is at 8.3 kpc. The number of pixels is a significant factor in the time taken to calculate the simulation. This number is determined by a spacing, which sets the spacing between adjacent rings and also the angular distance between pixels within a ring. For this toy model, the separation is 0.1 kpc, giving a rough pixel size of 0.01 kpc^2. For the actual model a smaller separation of 0.06 kpc (giving a pixel size of 0.0036 kpc^2) was used. The Solar System is 4.6 Gyr old while the Milky Way roughly 10 Gyr old. This means roughly 5 Gyr have to be tracked within the model. For this toy model, a timestep of 5 Myr over 100 iterations for a total time of 500 Myr was used. However, for the full model (model 2), a timestep of 50 Myr over 250 iterations for a total of 12.5 Gyr was tracked.
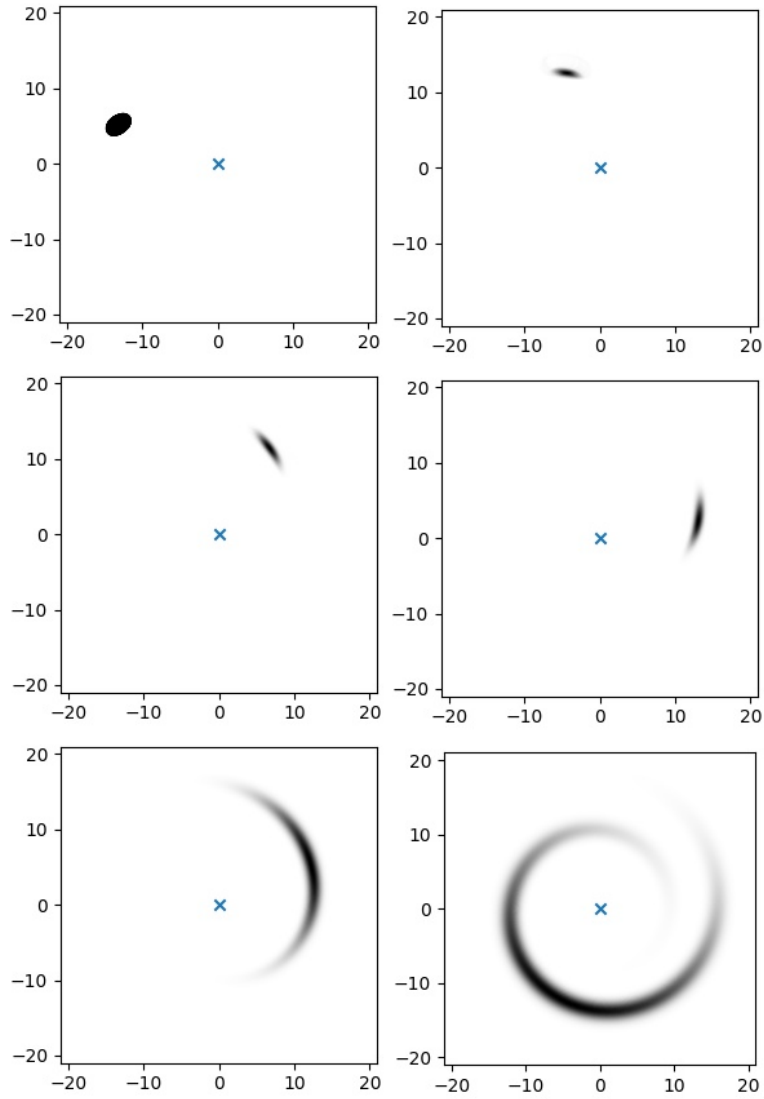
Fig. 13. *Diffusion from a single point with threshold distance of* 0.707 kpc. *This series of images shows the diffusion from a single point. They are the images of the Galaxy at various times* $(t = 0, 50, 100, 150, 500, 1000$ *kpc) after a NSM event. This image is made using model 1a. In this case, the timestep is* 50 Myr *and the diffusion constant is* 10 kpc^{2}Myr^{-1}. *Thus, the threshold distance for diffusion is* 0.707 kpc. *Note how the matter spreads azimuthally much faster than it does radially.*

4.1.2 Multiple events

To model the Galaxy at the rate of one NSM event per timestep would require prohibitively many timesteps[9]. Therefore multiple pixels were designated to be NSM events every timestep. This was done by choosing pixels at random. This means that the formation rate of NSM events is assumed to be constant over time and flat across the Galaxy.

---

[9]at a rate of 24.1 Myr^{-1}[27], this would mean roughly 40000 years per timestep. Thus would require 12500 timesteps for the 10 Gyr period
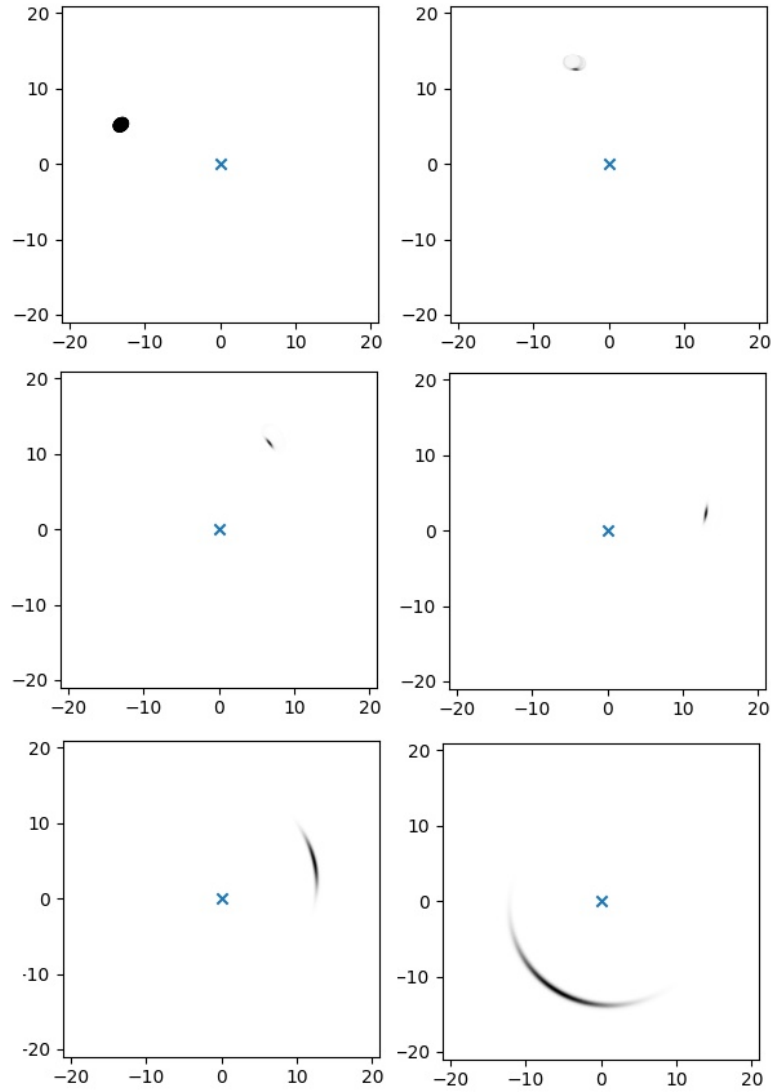
Fig. 14. *Diffusion from a single point with threshold distance of* 0.223 kpc. *This series of images shows the diffusion from a single point. They are the images of the Galaxy at various times* $(t = 0, 50, 100, 150, 500, 1000$ *kpc) after a NSM event. This image is made using model 1b. In this case, the timestep is* 50 Myr *and the diffusion constant is* 1 kpc^{2}Myr^{-1}. *Thus, the threshold distance for diffusion is* 0.223 kpc. *Compared to fig. 13, this has a smaller diffusion rate through the Galaxy, due to the smaller diffusion constant.*

4.2 Matter profile in a pixel

In figure 15, the amount of NSM matter in a pixel is shown (using the complete model: model 2). Of note, is the gradual increase in matter from the neutron star mergers. This gradual increase is interrupted by sudden spikes. These spikes occur when a neutron star merger is near to the pixel. The hypothesis runs that the Sun's composition was modified by one of these spikes during its formation.

The gradual linear increase can be seen especially clearly in figure 16. This is the mean value of the pixels throughout the Galaxy. Here, the spikes have been averaged out. Compare this to figure 17, which shows the standard deviation of the NSM matter amount throughout the Galaxy. The

36
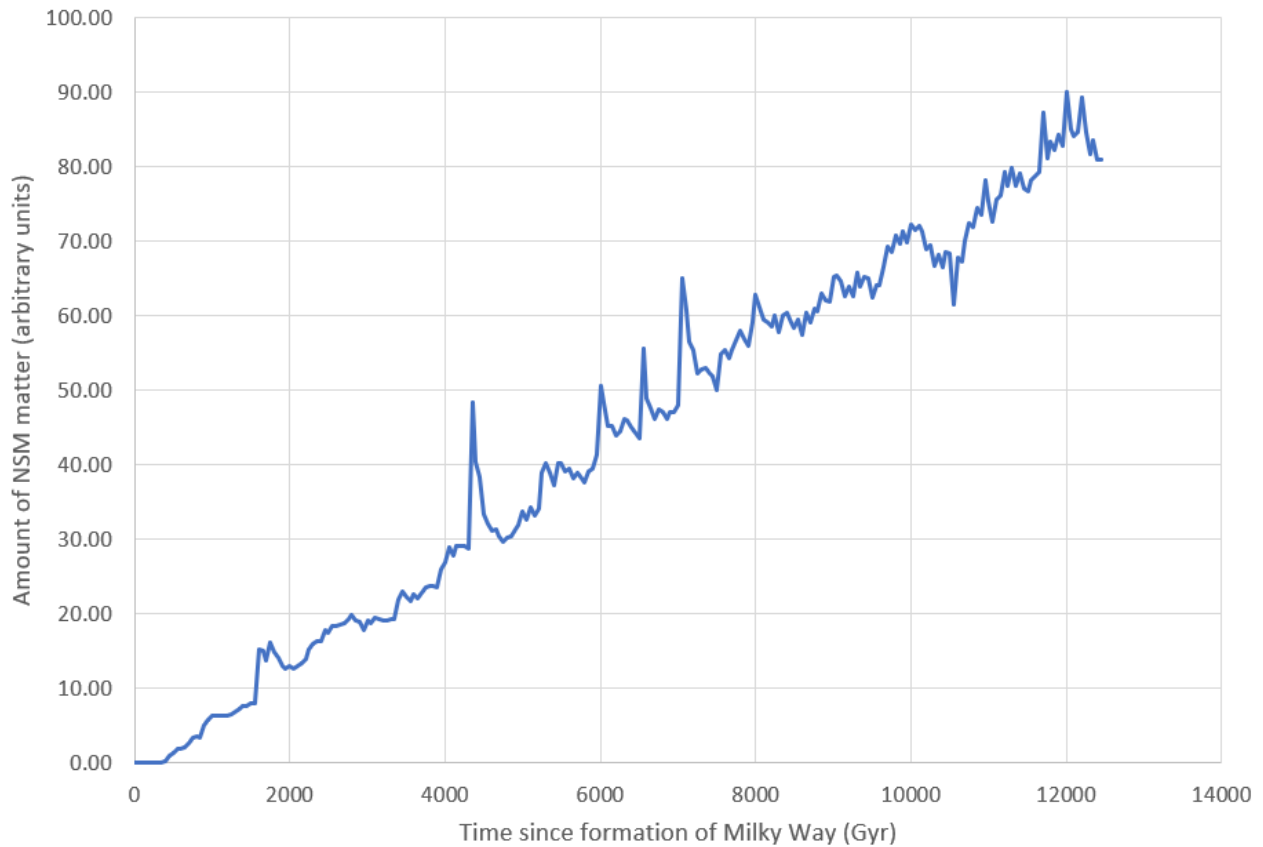
Fig. 15. *This figure shows the amount of neutron star matter in a pixel* 8.3 pc *from the centre. This is the distance from the centre of the Galaxy to the Sun. It uses arbitrary units for the y-axis. Of note is how the amount of matter in a pixel can be approximated by a linearly increasing value with occasional spikes in amount. This analysis is done on the complete model (model 2 in table 3).*

standard deviation grows slower than the mean. This means that the Galaxy becomes more more homogeneous over time.

4.3 Diffusion

Diffusion is modelled by distributing all the matter in a pixel amongst the pixels within a threshold distance. This distance is calculated by equation 4. Here d is the threshold distance (in kpc) and T is the timestep (in Myr). Due to the rotation, there is, effectively, two different diffusion rates: one azimuthal, the other radial. This can be seen in figure 13, which shows the diffusion from a single event. This is done by showing the Galaxy at $t = 0, 50, 100, 150, 500, 1000$ kpc.

4.4 Calculating a

a, as described in equation 2, is the fraction of the cometary composition that was injected. This was calculated by comparing the change in matter within a pixel over time, as seen in equation 5.
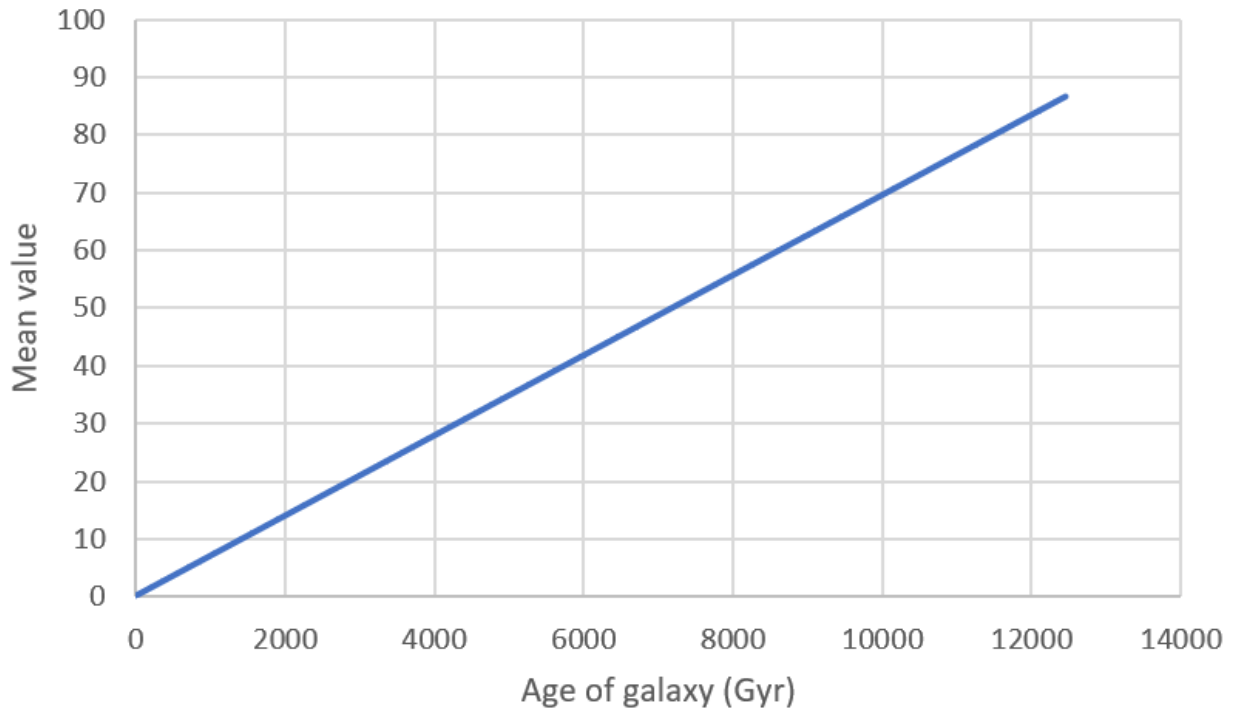
Fig. 16. *Mean amount of NSM matter among all the pixels in the Galaxy. Note how all the spikes seen in fig. 15 are averaged out, so only the overall linear increase can be seen. This analysis is done on the complete model (model 2 in table 3).*
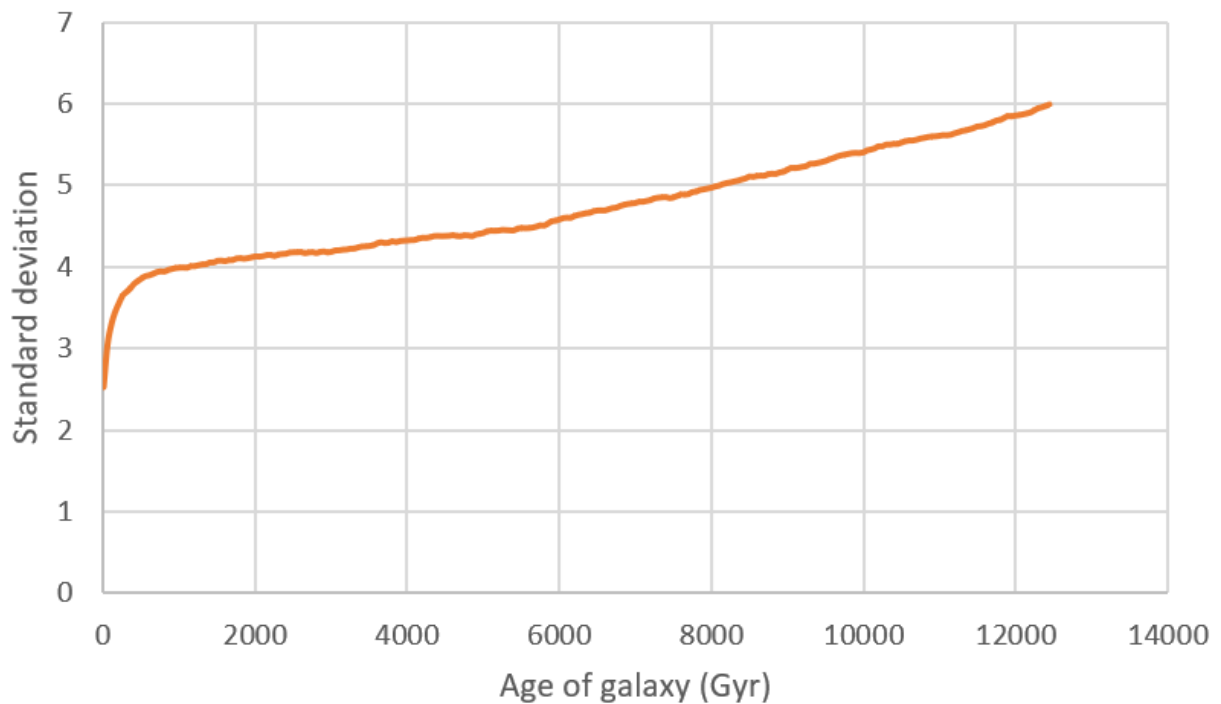
Fig. 17. *Standard deviation of the amount of NSM matter among the pixels. This characterises the size of the spikes seen in fig. 15. Note how this grows much slower than the average (fig. 16). This analysis is done on the complete model (model 2 in table 3).*
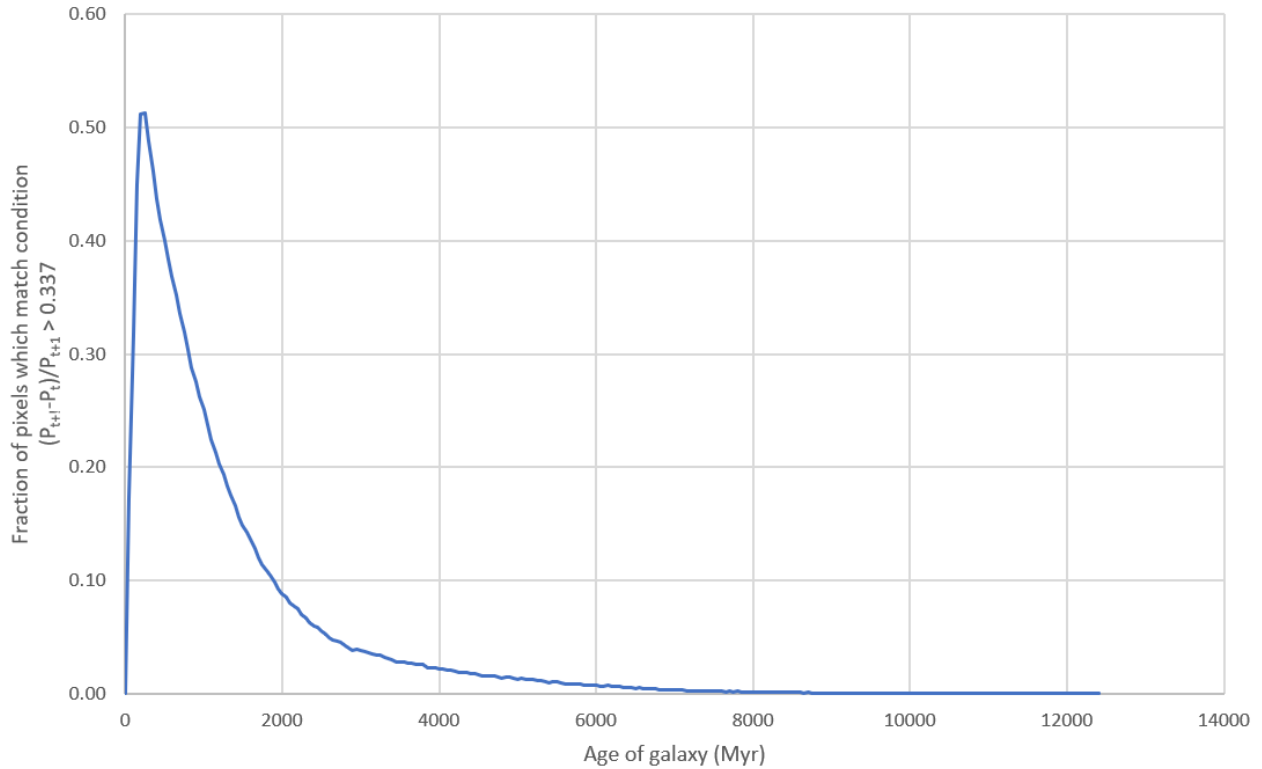
Fig. 18. *This shows the fraction of pixels within the radii of 5-15 kpc where $\frac{P_t - P_{t+1}}{P_t} > 0.34$. P_t is amount of matter in a pixel at time t. The threshold of 0.34 comes from $a > 0.34$. At early times, there is a strong increase. This is due to the new addition of r-process material. Over time, this fraction steadily approaches zero. This is due to the steadily increasing amount of NSM matter. This increased baseline means that each individual NSM makes a smaller fractional change within a pixel. At the time of the Solar System's formation (roughly 5 Gyr from the start of the Milky Way), 1.3% of the pixels fit this parameter. This analysis is done on the complete model (model 2 in table 3).*

This is plotted in figure 18. From this, the model predicts that, at the time of the Solar System's formation at 5 Gyr, 1.3% of pixels match the 97.5% confidence conditions.

This model suggests that conditions which would produce the Xe composition of the Solar System are exceedingly rare. By considering the range of error in a, the Solar System becomes even more rare. As can be seen in figure 10, most of the variability in a comes from the imprecise measurement of the cometary composition. By considering the 2σ errors, the value of $a > 0.34$ was found with 97.5% confidence. By instead considering the average values, we get $a > 0.611$. This means that even fewer pixels match the valid conditions.

Comparing the model what is seen in the Solar System suggests that the Solar System was enriched in a very rare event. This suggests that the model is incomplete. This implications and significance of this result will be discussed in section 4.6.

Note that this is a closed-box model: no material enters or exits the Galaxy. For the Milky Way, there is a constant input of non r-process material. This make the Milky Way age slower than it does within this model[31].

4.5 Implications of a

As can be seen in figure 18, the conditions which would produce the Xe composition of the Solar System are exceedingly rare. One must also consider the fact that the calculated value for a is already a lower limit. This is because $a = \frac{S-C}{S-A}$, as described in equation 5. Removing the assumption that the injected composition has no ^{136}Xe means that the calculated value for a will be higher, resulting in even fewer pixels that match the conditions set by the value of a.

This leads to two possible conclusions: 1) the Solar System is indeed very rare or 2) the assumptions made by the model mean that the Solar System is more probable than the model predicts.

4.6 Limitations of the model

This model focuses on the diffusion of NSM ejecta. This assumes that the variation in the xenon composition within the Solar System was caused by a late injection of NSM matter. This variation is seen in figure 10. To characterise this variation two end members were chosen: the solar (Xe-SW) compositions and a hypothetical injected composition (Xe-NSM). Xe-SW was chosen to be the majority composition of the Solar System. To this, Xe-NSM is added till Xe-67P/CG can be formed.

Figure 10, shows the ^{136}Xe/^{132}Xe ratio against the ^{134}Xe/^{132}Xe ratio of the various compositions within the Solar System once the s-process composition is subtracted. Since, this graph plots a straight line, the existence of two r-processes is inferred. The composition resulting from each r-process would form the extremities of the line with all the compositions being a particular mix of these extreme compositions. Each of these pure compositions are called the end members.

Presumably, the xenon composition ejected by the neutron star mergers would be a mix of the r-process but for this analysis, it is assumed that Xe-NSM produces a composition with no ^{136}Xe. This minimises the amount of matter needed to change the Xe-SW to match Xe-67P/CG. Thus, an upper limit for a can be calculated.

This model uses several assumptions to work. One of them is that the cometary composition formed after the solar composition. This model does not consider the possibility that the cometary composition is older than the solar composition.

This also relies on the existence of two r-processes and that neutron star mergers are a site at which on of these r-processes happen. This has some supporting evidence but is not definitively proven[22][32]. In addition to this, it assumes that all NSM events produce this new r-process. If this assumption is incorrect, the model can be corrected by varying and the amount of NSM matter created by each NSM event.

The s-process is the other main way that heavy isotopes are created. It is made in low and intermediate mass stars in the AGB stage. The enrichment due to the s-process is considered in section

2.2.3. However, this assumes the s-process enriches at constant rate. However, Battistini et al.[33] and Spina et al.[34] show that the rate of the s- and r-process enrichment vary over the course of galactic history. This is due to the enriching events occurring on different timescales. Following a burst of star formation, the r-process supernovae occur within 10 Myr, the s-process occurs between 100 Myr and 1 Gyr and the neutron star mergers would occur later. The exact timescale of neutron star mergers is unknown but it must occur with some delay after the supernovae.

A more sophisticated model would include details of the relative formation rates of the s- and r-processes to get accurate ratios of ^{136}Xe/^{132}Xe. This is because ^{132}Xe is created by both the s- and r-process. This advanced model would need the star formation history as well as timescales for stellar evolution (to estimate an accurate delay time between formation and matter ejection) for different stellar mass ranges.

This would also correct the assumption within the current model of a flat star formation rate and distribution. Currently, there is no variation in the NSM rate with time. It is also assumed that the NSM rate is constant over the galactic plane. They are instead concentrated in the Galactic plane and towards the centre of the Galaxy. To correct for this, population estimates of neutron star mergers can be used to create a model that includes details about galactic structure and history. De Cia et al.[31] used a 3D model of the Galaxy and a similar method can be adapted for this.

Further assumptions have been made regarding the mixing of r-process matter. Currently, the matter within a pixel is distributed evenly amongst pixels within a threshold distance. This threshold distance is calculated such that the diffusion speed is kept constant irrespective of the timestep. A more advanced model can consider a mixing fraction where only a part of the matter in a pixel is distributed out to the other pixels. Beniamini and Hotokezada[30] consider a similar model with a high turbulent velocity but a low mixing fraction. This is in comparison to the current model, which has a low turbulent velocity but a high mixing fraction. A more sophisticated model with a higher turbulent velocity and lower mixing fraction will likely produce similar results.

Another assumption with the mixing is that the interstellar medium is assumed to be of a single (gaseous) component. The solid phase component (dust) may evolve differently. Presolar grains have shown that some dust grains formed in different locations at different times and kept the composition of their origin. This time delay is not included in the model and it is important because the planets and comets in part evolve from the solid phase.

Currently, the pixels have a separation of 0.06 kpc and a single timestep is 50 Myr. In the current model diffusion occurs at a velocity of roughly 1 kms^{-1}. It is worth noting that diffusion is accelerated by galactic rotation forming arcs. This was not considered in the paper by Beniamini and Hotokezaka[30]. A full model will include all these aforementioned effects.

The resolution of the model is not fine enough to fully capture the injection of material into the Solar System. The delay between the formation of the Sun and the condensation of the rocky planets is roughly 5 Myr[35]. This is faster than the time resolution of the model. In addition, the Sun's

influence extends up to roughly a quarter of a parsec. From this it is clear that the model cannot capture the interior details of the Solar System. The current resolution was used due to resource constraints with computing power as computation time scales with $\mathcal{O}(n^2)$ with n being the number of pixels. In addition, the computation time scales linearly with the number of timesteps. Some of these requirements can be sidestepped by only considering the area around the Sun at the Solar System's time of formation.

5 Discussion

The results of the model suggest that the Solar System is very rare. Now we discuss factors not included in the model which may modify this conclusion.

First of these, is that the model is a closed-box. This means that no in-fall of matter into the Galaxy is considered. As described by De Cia et al.[31], modelling the in-falling matter makes the Galaxy age slower compared to the closed-box model. However, this has limited effect on the model prediction. As can be seen in figure 18 even halving simulation age to 2 Gyr only raises the fraction of matching pixels to 5.5%.

A much more significant effect comes from the mixing model used. Currently, it is assumed that the composition of the comets is from a modified solar composition. Of the total Solar System mass, the comets and similar outer Solar System object form a miniscule fraction. Currently, it is assumed that the NSM ejecta are dispersed throughout the Solar System but only preserved in the outer Solar System. Instead, it can be assumed that the NSM ejecta only affected a very small part of the Solar System. This means that instead of considering pixels where $\frac{P_t - P_{t+s}}{P_t} > 0.34$, we instead consider pixels where the fractional change is > 0. This can be seen in figure 19. This shows that now 53% of pixels now fit the conditions. This is an upper limit, as it assumes that all of the injected matter is condensed onto the outer Solar System and that this part of the Solar System is such a small portion that any NSM injection injects enough matter to create the resultant compositions.

The Sun is assumed to be the oldest component of the Solar System. It formed first, during the initial collapse of the proto-solar cloud. It also accounts for the large majority of the mass ($> 99\%$) of the Solar System. The comets formed later from the residual mass. The comets have lower ^{136}Xe abundance. Therefore, a late-time injection of ^{136}Xe-poor matter is considered and this is assumed to come from NSM.

There is the further assumption that the solar composition is older than the cometary composition. There is also the possibility that the comets are from a composition that is older than the Solar System. Though the comets themselves formed during the Solar System formation, it is possible that they formed around presolar grains, which have preserved their composition.

There are now two possible timelines of events:

1. The Sun formed first

   (a) Some event injected new matter to the outer Solar System

      i. The comets form from this altered composition

2. The comets formed first

   (a) Some event injected new matter to change the composition of the interstellar matter (ISM)

      i. The Sun and the rest of the Solar System formed from the ISM with the altered composition

Of these two possible sequence of events, the first is what is considered in the model. This requires an event that injects a ^{136}Xe-poor composition. This event is taken to be a neutron star merger. For the other sequence of events, a ^{136}Xe-rich is instead injected. The difference between the two situations is that the second requires a much higher mass input.
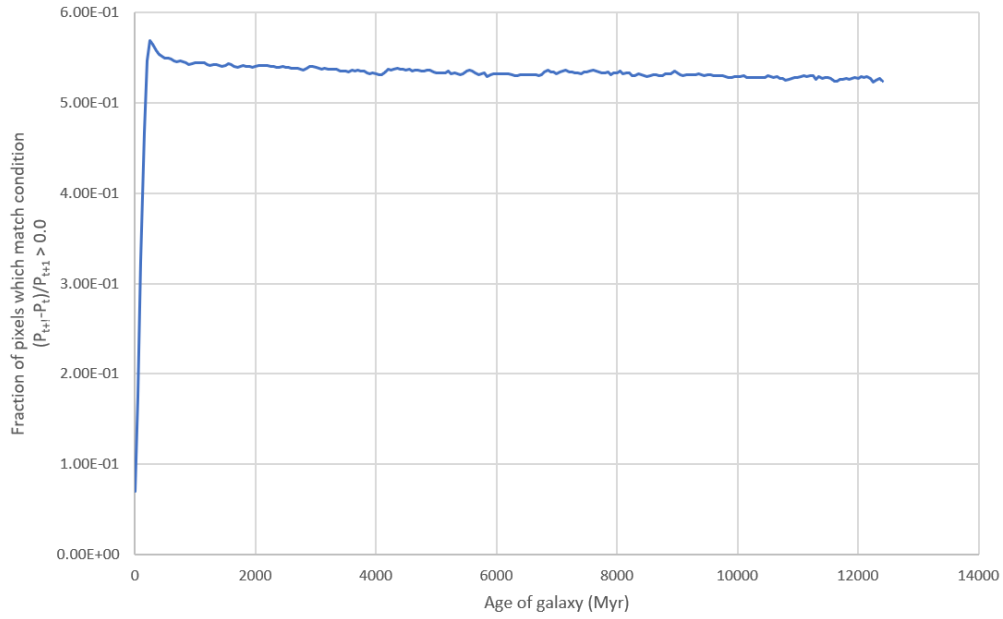
(a) $a = 0.0$
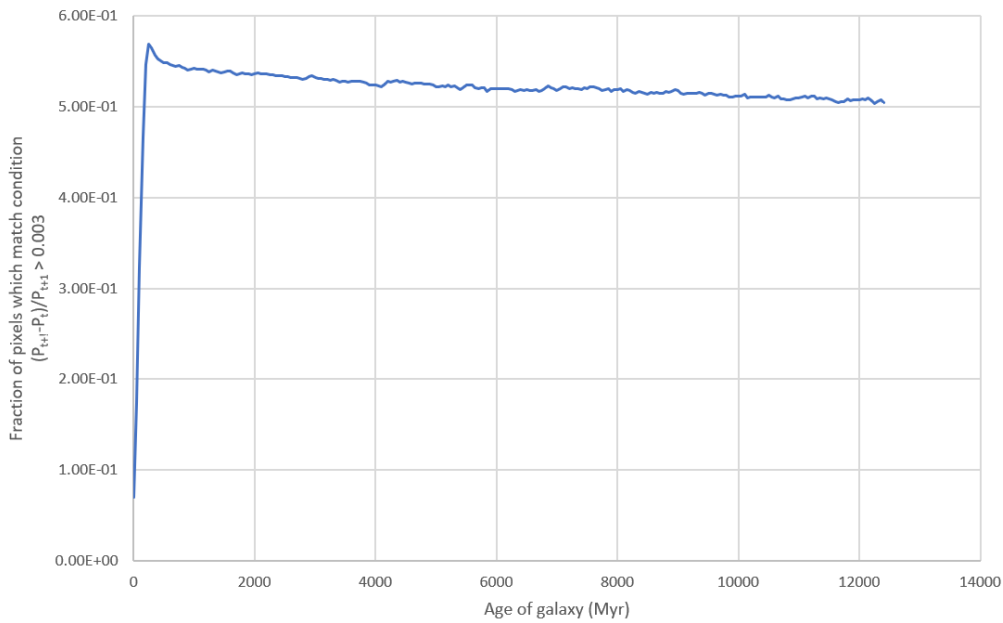
(b) $a = 0.003$

Fig. 19. *These figures show the effect of considering various values of a ($a = 0.0$, $a = 0.003$, $a = 0.03$, $a = 0.34$ respectively). $a = 0.34$ is calculated by using the solar and cometary compositions. At the age of 5 Gyr, 1.3% of all pixels match the condition that $a > 0.34$. By considering that only a small fraction of the matter of the Solar System is in the comets and similar outer Solar System bodies, smaller values of a can be considered. The minimum value of $a = 0.0$ gives 53% of pixels fit the conditions. At higher values of a, the fraction of matching pixels decrease faster with time. This analysis is done on the complete model (model 2 in table 3).*

(c) $a = 0.03$

(d) $a = 0.34$

Fig. 19. *(cont.) These figures show the effect of considering various values of a ($a = 0.0$, $a = 0.003$, $a = 0.03$, $a = 0.34$ respectively). $a = 0.34$ is calculated by using the solar and cometary compositions. At the age of 5 Gyr, 1.3% of all pixels match the condition that $a > 0.34$. By considering that only a small fraction of the matter of the Solar System is in the comets and similar outer Solar System bodies, smaller values of a can be considered. The minimum value of $a = 0.0$ gives 53% of pixels fit the conditions. At higher values of a, the fraction of matching pixels decrease faster with time. This analysis is done on the complete model (model 2 in table 3).*

6 Conclusions and future work

6.1 Summary

By measuring xenon compositions across the Solar System, they can be seen to vary. The isotopic ratios are different between the Sun, planets, asteroids and comets. This can be seen in figure 9. The cause of this variation is not understood and persists even when considering mass fractionation. This suggests that the compositional variation is due to differences in origin.

There are two main routes by which nucleosynthesis can create xenon. These are the s- and r-processes. The s- process adds neutron to the nucleus slower than the β decay rate. This results in a stepwise motion through the nuclide chart around the region of stability. The r-process occurs in regions where the density of neutrons is sufficiently high to add neutrons to the nucleus faster than the β decay rate. This creates neutron-rich isotopes which subsequently β-decay.

Because the s-process runs exclusively through isotopes near the stable region, its contribution can be calculated and thus removed from the xenon compositions. The r-process is inferred to be the remainder in a xenon composition once the s-process contribution is subtracted.

In figure 10, the resulting r-process xenon isotopic ratios throughout the Solar System are found to lie on a straight line. This is best explained by two distinct nucleosynthetic processes, whose overall effect has been called the r-process (hereby called 136-rich and 136-poor compositions). This is backed-up by recent research[12][14] that suggests that neutron star mergers (NSM) are an alternate source of r-process material compared to the traditionally regarded source of core-collapse supernovae.

This model considers the possibility that the variation of the r-process elements is due to a late-injection of NSM ejecta. This changes some of the material from the predominant solar composition to the 136-poor cometary composition. Due to the difference in rates between NSM events (24.1 Myr^{-1}[27]) and supernovae events (0.0163 yr^{-1}[26]), the r-process material from supernovae is considered to provide a constant background, while the r-process material from NSM is considered to be stochastic and to cause variations both over time and across the Galaxy.

The model calculates the abundance variations caused by individual NSM events in their local environment. Thus it gives a likelihood of a region in space having a matching mix of r-process material as the Solar System. The model consists of a simplified 2D Galaxy made of pixels. These pixels track the NSM ejecta within them. This ejecta is then tracked as it diffuses through the rotating Galaxy.

Using equation 1, the cometary composition (C) can be thought of as a mix between the solar composition (S) and the injected composition (A). a is the fraction of the cometary composition that comes from the injected composition. Since the cometary composition has less ^{136}Xe than the

solar composition, it can be inferred that A is 136-poor. a is minimised when the injected composition has no ^{136}Xe. From the measured solar and cometary composition, we find for that case $a = 0.34$.

Within the model a corresponds to a fractional change within a pixel over a timestep. This fractional change is calculated for each pixel and the fraction of pixels that have a fractional change above 0.34 is plotted in figure 18.

6.2 Conclusion

Figure 18, predicts that that only 1.3% of all pixels at a galactic age of 5 Gyr have a fractional change greater than 0.34. This suggests that the compositional variation seen in the Solar System is extremely rare.

This rarity can be partly attributed to the rarity of NSM events. Each individual event has a significant effect on nearby pixels as can be seen in figure 15, which tracks the NSM matter in a pixel at a similar distance to the galactic centre as the Sun. The figure shows a steady increase in NSM matter punctuated by spikes caused by a nearby NSM event. These spikes can contribute as much as 40% of the matter within a single pixel.

The diffusion of the NSM ejecta is amplified azimuthally due to the rotation of the Galaxy. This can be seen in figure 13. This figure also illustrates the effect of the varying rotation rate. Closer to the centre, there is a faster angular velocity, resulting in even faster dffusion. This results in the diffusion moving along a spiral pattern.

6.3 Future work

The main area in which the model is limited is with its fidelity. Currently, each pixel is many times bigger than the size of the Solar System and the size of the timestep is many times longer than the time taken for the Solar System to form. With more time and more computational resources, higher fidelity in this regard could be achieved.

Further, some of the assumptions and simplifications that were made can be re-examined. Of note is the in-fall rate of new matter. In addition, considerations can be made to match the formation rates of the stars. This will mean using a variable rate of NSM events. Similarly, the diffusion calculation can be made more sophisticated. For example, the diffusion model could have an exponential decay. Another example is running a similar model with supernovae included instead of a constant background.

This model can also be adjusted to use other isotopes with similar heterogeneities.

Separate to improvements in the model, better measurements of the Xe compositions can be made. Of note is the cometary xenon compositions like Xe-67P/CG. Currently, only the comet 67P/Churymov-Gerasimenko has had its xenon composition measured. This means that there are significant errors with the cometary xenon composition. There is the possibility that the 67P/CG comet may have originated from a poorly mixed region of the Solar System. This drastically loosens the constraints imposed by the model (from 1.3% to 53% of the ISM with suitable conditions). Further missions to various comets (prefereably sample return missions so isotope compositions can be measured) will be required before these measurement errors can be minimised and multiple parts of the Solar System can be sampled.

New data can be expected from the Hayabusa 2 mission. It has returned a sample from asteroid Ryugu in November and will visit two more asteroids in the coming ten years[36].

Better calculations of the r- and s-process contributions to xenon compositions using finer models of the neutron addition and photo-disintegration will improve the data upon which this model is based on. Currently, the r-process composition must be inferred by subtracting out the s-process. Directly calculating the r-process contribution will also allow investigations into the conditions under which different regimes of the r-process occur.

References

[1] C. Christensen, A. Nielsen, A. Bahnsen, W. Brown, and B. Rustad, "The half-life of the free neutron," *Physics Letters B*, vol. 26, no. 1, pp. 11–13, 1967. DOI: `10.1016/0370-2693(67)90532-1`.

[2] *Hertzsrpung-russell diagram*, 2007. [Online]. Available: `https://www.eso.org/public/images/eso0728c/`.

[3] E. M. Burbidge, G. R. Burbidge, W. A. Fowler, and F. Hoyle, "Synthesis of the elements in stars," *Reviews of Modern Physics*, vol. 29, no. 4, pp. 547–650, 1957. DOI: `10.1103/revmodphys.29.547`.

[4] *Nuclear binding energy*, 2020. [Online]. Available: `https://phys.libretexts.org/Bookshelves/University_Physics/Book%5C%3A_University_Physics_(OpenStax)/Book%5C%3A_University_Physics_III_-`

`_Optics_and_Modern_Physics_(OpenStax)/10%5C%3A__Nuclear_``Physics/10.03%5C%3A_Nuclear_Binding_Energy`.

[5]   A. Trinquier, J.-L. Birck, and C. J. Allegre, "Widespread 54cr heterogeneity in the inner solar system," *The Astrophysical Journal*, vol. 655, no. 2, pp. 1179–1185, 2007. DOI: `10.1086/510360`.

[6]   A. P. Boss, "Evolution of the solar nebula. viii. spatial and temporal heterogeneity of short-lived radioisotopes and stable oxygen isotopes," *The Astrophysical Journal*, vol. 660, no. 2, pp. 1707–1714, 2007. DOI: `10.1086/513184`.

[7]   N. Dauphas and E. A. Schauble, "Mass fractionation laws, mass-independent effects, and isotopic anomalies," *Annual Review of Earth and Planetary Sciences*, vol. 44, no. 1, pp. 709–783, 2016. DOI: `10.1146/annurev-earth-060115-012157`.

[8]   B. Marty, K. Altwegg, H. Balsiger, A. Bar-Nun, D. V. Bekaert, J.-J. Berthelier, A. Bieler, C. Briois, U. Calmonte, and M. e. a. Combi, "Xenon isotopes in 67p/churyumov-gerasimenko show that comets contributed to earth's atmosphere," *Science*, vol. 356, no. 6342, pp. 1069–1072, 2017. DOI: `10.1126/science.aal3496`.

[9]   E. Simpson, *Colourful nuclide chart*, 2021. [Online]. Available: `https://people.physics.anu.edu.au/~ecs103/chart/`.

[10] D. D. Clayton and R. A. Ward, "S-process studies - xenon and krypton isotopic abundances," *The Astrophysical Journal*, vol. 224, p. 1000, 1978. DOI: `10.1086/156449`.

[11] L. Girardi, A. Bressan, G. Bertelli, and C. Chiosi, "Evolutionary tracks and isochrones for low- and intermediate-mass stars: From 0.15 to 7 solar mass, and from z=0.0004 to 0.03," *Astronomy and Astrophysics Supplement Series*, vol. 141, no. 3, pp. 371–383, 2000. DOI: `10.1051/aas:2000126`.

[12] M. R. Drout, A. L. Piro, B. J. Shappee, C. D. Kilpatrick, J. D. Simon, C. Contreras, D. A. Coulter, R. J. Foley, M. R. Siebert, and N. e. a. Morrell, "Light curves of the neutron star merger gw170817/sss17a: Implications for r-process nucleosynthesis," *Science*, vol. 358, no. 6370, pp. 1570–1574, 2017. DOI: `10.1126/science.aaq0049`. [Online]. Available: `https://arxiv.org/abs/1710.05443`.

[13] B. J. Shappee, J. D. Simon, M. R. Drout, A. L. Piro, N. Morrell, J. L. Prieto, D. Kasen, T. W.-S. Holoien, J. A. Kollmeier, and D. D. e. a. Kelson, "Early spectra of the gravitational wave source gw170817: Evolution of a neutron star merger," *Science*, vol. 358, no. 6370, pp. 1574–1578, 2017. DOI: `10.1126/science.aaq0186`. [Online]. Available: `https://arxiv.org/abs/1710.05432`.

[14] K. Hotokezaka, P. Beniamini, and T. Piran, "Neutron star mergers as sites of r-process nucleosynthesis and short gamma-ray bursts," *International Journal of Modern Physics D*, vol. 27, no. 13, p. 1 842 005, 2018. DOI: `10.1142/s0218271818420051`. [Online]. Available: `https://doi.org/10.1142/S0218271818420051`.

[15] E. Aprile, J. Aalbers, and et al., "Observation of two-neutrino double electron capture in xe-124 with xenon1t," *NATURE*, vol. 568, no. 7753, pp. 532+, 2019, ISSN: 0028-0836. DOI: `10.1038/s41586-019-1124-4`.

[16] J. J. Cowan, C. Sneden, J. E. Lawler, A. Aprahamian, M. Wiescher, K. Langanke, G. Martínez-Pinedo, and F.-K. Thielemann, "Origin of the heaviest elements: The rapid neutron-capture process," *Reviews of Modern Physics*, vol. 93, no. 1, 2021. DOI: `10.1103/revmodphys.93.015002`.

[17] C. Kobayashi, A. I. Karakas, and M. Lugaro, "The origin of elements from carbon to uranium," *The Astrophysical Journal*, vol. 900, no. 2, p. 179, 2020. DOI: 10.3847/1538-4357/abae65.

[18] A. Meshik, C. Hohenberg, O. Pravdivtseva, and D. Burnett, "Heavy noble gases in solar wind delivered by genesis mission," *Geochimica et Cosmochimica Acta*, vol. 127, pp. 326–347, 2014. DOI: 10.1016/j.gca.2013.11.030.

[19] T. Peters, S. Zhukovska, T. Naab, P. Girichidis, S. Walch, S. C. O. Glover, R. S. Klessen, P. C. Clark, and D. Seifried, "The turbulent life of dust grains in the supernova-driven, multiphase interstellar medium," *Monthly Notices of the Royal Astronomical Society*, vol. 467, no. 4, pp. 4322–4342, 2017. DOI: 10.1093/mnras/stx341.

[20] G. Avice, M. Moreira, and J. D. Gilmour, "Xenon isotopes identify large-scale nucleosynthetic heterogeneities across the solar system," *ASTROPHYSICAL JOURNAL*, vol. 889, no. 1, 2020, ISSN: 0004-637X. DOI: 10.3847/1538-4357/ab5f0c.

[21] D. S. Burnett and G. S. Team, "Solar composition from the genesis discovery mission," *Proceedings of the National Academy of Sciences*, vol. 108, no. 48, pp. 19 147–19 151, 2011. DOI: 10.1073/pnas.1014877108.

[22] K. Terada, K. Itoh, H. Hidaka, T. Yoshida, N. Iwamoto, W. Aoki, and I. Williams, "Eu isotope measurements on single sic grains from the murchison meteorite: A new probe of s-process conditions in parent asymptotic giant branch stars," *New Astronomy Reviews*, vol. 50, no. 7-8, pp. 582–586, 2006. DOI: 10.1016/j.newar.2006.06.006.

[23] R. S. Lewis, S. Amari, and E. Anders, "Interstellar grains in meteorites: Ii. sic and its noble gases," *Geochimica et Cosmochimica Acta*, vol. 58, no. 1, pp. 471–494, 1994. DOI: 10.1016/0016-7037(94)90478-2.

[24] J. D. Gilmour and G. Turner, "Constraints on nucleosynthesis from xenon isotopes in presolar material," *The Astrophysical Journal*, vol. 657, no. 1, pp. 600–608, 2007. DOI: 10.1086/510881. [Online]. Available: `https://iopscience.iop.org/article/10.1086/510881`.

[25] G. J. Wasserburg, M. Busso, and R. Gallino, "Abundances of actinides and short-lived nonactinides in the interstellar medium: Diverse supernova sources for the [ital]r[/ital]-processes," *The Astrophysical Journal*, vol. 466, no. 2, pp. L109–L113, 1996. DOI: `10.1086/310177`.

[26] K. Rozwadowska, F. Vissani, and E. Cappellaro, "On the rate of core collapse supernovae in the milky way," *New Astronomy*, vol. 83, p. 101 498, 2020. DOI: `10.1016/j.newast.2020.101498`.

[27] M. Chruslinska, K. Belczynski, J. Klencki, and M. Benacquista, "Double neutron stars: Merger rates revisited," *Monthly Notices of the Royal Astronomical Society*, vol. 474, no. 3, pp. 2937–2958, 2018. DOI: `10.1093/mnras/stx2923`.

[28] C. Winteler, R. Käppeli, A. Perego, A. Arcones, N. Vasset, N. Nishimura, M. Liebendörfer, and F.-K. Thielemann, "Magnetorotationally driven supernovae as the origin of early galaxy r-process elements?" *The Astrophysical Journal*, vol. 750, no. 1, p. L22, 2012. DOI: `10.1088/2041-8205/750/1/l22`.

[29] M. J. Reid, K. M. Menten, A. Brunthaler, X. W. Zheng, T. M. Dame, Y. Xu, Y. Wu, B. Zhang, A. Sanna, M. Sato, K. Hachisuka, Y. K. Choi, K. Immer, L. Moscadelli, K. L. J. Rygl, and A. Bartkiewicz, "Trigonometric parallaxes of high mass star forming regions: The structure and kinematics of the milky way," *The Astrophysical Journal*, vol. 783, no. 2, p. 130, 2014. DOI: `10.1088/0004-637x/783/2/130`.

[30] P. Beniamini and K. Hotokezaka, "Turbulent mixing of r-process elements in the milky way," *Monthly Notices of the Royal Astronomical Society*, vol. 496, no. 2, pp. 1891–1901, 2020. DOI: 10.1093/mnras/staa1690.

[31] A. De Cia, E. B. Jenkins, A. J. Fox, C. Ledoux, T. Ramburth-Hurt, C. Konstantopoulou, P. Petitjean, and J.-K. Krogager, "Large metallicity variations in the galactic interstellar medium," *Nature*, vol. 597, no. 7875, pp. 206–208, 2021. DOI: 10.1038/s41586-021-03780-0.

[32] O. Just, A. Bauswein, R. A. Pulpillo, S. Goriely, and H.-T. Janka, "Comprehensive nucleosynthesis analysis for ejecta of compact binary mergers," *Monthly Notices of the Royal Astronomical Society*, vol. 448, no. 1, pp. 541–567, 2015. DOI: 10.1093/mnras/stv009.

[33] C. Battistini and T. Bensby, "The origin and evolution ofr- ands-process elements in the milky way stellar disk," *Astronomy & Astrophysics*, vol. 586, A49, 2016. DOI: 10.1051/0004-6361/201527385.

[34] L. Spina, J. Meléndez, A. I. Karakas, L. d. Santos, M. Bedell, M. Asplund, I. Ramírez, D. Yong, A. Alves-Brito, and J. L. Bean, "The temporal evolution of neutron-capture elements in the galactic discs," *Monthly Notices of the Royal Astronomical Society*, 2017. DOI: 10.1093/mnras/stx2938.

[35] Q. Yin, S. B. Jacobsen, K. Yamashita, J. Blichert-Toft, P. Télouk, and F. Albarède, "A short timescale for terrestrial planet formation from hf–w chronometry of meteorites," *Nature*, vol. 418, no. 6901, pp. 949–952, 2002. DOI: 10.1038/nature00995.

[36] M. Hirabayashi, Y. Mimasu, N. Sakatani, S. Watanabe, Y. Tsuda, T. Saiki, S. Kikuchi, T. Kouyama, M. Yoshikawa, and S. e. a. Tanaka, "Hayabusa2 extended mission: New voyage to rendezvous with a small asteroid rotating with a

short period," *Advances in Space Research*, vol. 68, no. 3, pp. 1533–1555, 2021. DOI: `10.1016/j.asr.2021.03.030`.

[37]   R. O. Pepin, "On the isotopic composition of primordial xenon in terrestrial planet atmospheres," *Space Science Reviews*, vol. 92, no. 1/2, pp. 371–395, 2000. DOI: `10.1023/a:1005236405730`.

[38]   ——, "On the origin and early evolution of terrestrial planet atmospheres and meteoritic volatiles," *Icarus*, vol. 92, no. 1, pp. 2–79, 1991. DOI: `10.1016/0019-1035(91)90036-s`.

Appendices

A Project outline

Understand xenon isotope variations across the Solar System in the context of current theories of nucleosynthesis and star forming processes.

B Risk assessment

This project was done entirely remotely. Therefore the physical laboratories were not accessed.

C Xenon composition data

Table 4. The raw data for the xenon compositions measured throughout the Solar System.

Xe composition	Source	124	126	128	129	130	131	132	134	136
Xe-Air	[37]	2.337±0.007	2.18±0.0011	47.146±0.047	649.58±0.58	100±	521.27±0.59	660.68±0.53	256.28±0.37	217.63±0.22
Xe-U	[37]	2.928±0.01	2.534±0.013	50.83±0.006	628.6±0.6	100±	499.6±0.6	604.7±0.6	212.6±0.4	165.7±0.3
Xe-Q	[37]	2.843±0.026	2.505±0.02	50.81±0.22	637.5±3.6	100±	504.6±2.2	615.4±1.9	234±0.9	195.7±0.9
Xe-H	[38]	-	-	-	-	-	7.3±5.2	24.9±1.8	71.23±0.78	100±
Xe-SW	[37]	0.00491±0.00007	0.00416±0.00009	0.0842±0.0003	1.0405±0.001	0.165±0.0004	0.8256±0.0012	1±	0.3691±0.0007	0.3001±0.0006
Xe-SW	[37]	2.3±0.26	2.1±	47.3±1.4	1556±8	100±	518±3.4	652.9±4.2	258.5±2.2	226.9±1.6
Xe-SW	[18]	-	-	0.076±0.021	1.398±0.122	0.184±0.032	0.846±0.09	1±	0.238±0.049	0.116±0.04
Xe-Mars	[37]	-	-	0.212±0.004	0.105±0.03	0.48±0.01	0.184±0.018	1±	0.013±0.005	-
Xe-Mars	[37]	2.3±0.26	2.1±	47.3±1.4	1556±8	100±	518±3.4	652.9±4.2	258.5±2.2	226.9±1.6
Xe-67P/CG	[8]	-	-	0.076±0.021	1.398±0.122	0.184±0.032	0.846±0.09	1±	0.238±0.049	0.116±0.04
Xe-s	[24]	-0.00065±0.00008	-0.0002±0.0001	0.212±0.004	0.105±0.03	0.48±0.01	0.184±0.018	1±	0.013±0.005	0±

D Code

Attached below is the code used to run the model.

```python
import numpy as np
import matplotlib.pyplot as plt
import copy
import os


def make_galaxy(inner_radius, outer_radius, radius_step):
    # This makes an empty galaxy with the pixels evenly spaced out
    # this is in the form of a list of lists
    #      each sublist is of the form:
    #      [radial coordinate, angular coordinate, NSM matter, 0.0}
    #      the final item in the sublist is as yet unused

    # make a list of radii
    radii = np.arange(inner_radius, outer_radius, radius_step)
    # calculate the size of the pixels from the distance between radii
    pixel_radial_size = abs(radii[0] - radii[1])

    full_coord_list = []
    for i, r in enumerate(radii):
        # each radius corresponds to a ring

        # find angular distance such that the distance azimuthally is the same
    as the distance between radii
        # note that the angle is adjusted so that there are a whole number of
    pixels along a ring
        angle_change = 2 * np.pi / round(2 * np.pi * r / pixel_radial_size)

        current_coord = -2*np.pi
        coord_list = []
        while current_coord < 0:
            coord_list.append([r, current_coord, 0., 0.])
            current_coord += angle_change
        full_coord_list.extend(coord_list)
    return np.array(full_coord_list)


```

```python
36  def rotate_galaxy(coordinates, timestep):
37      # This rotates a galaxy according to the following equations:
38      #     for pixels with radial coordinate < 5kpc:
39      #         rotation [radian] = timestep [Myr] * 48 [km s^-1 kpc^-1] *
    conversion factor [kpc s km^-1 Myr^-1]
40      #     for pixels with radial coordinate > 5kpc:
41      #         rotation [radian] = timestep [Myr] * 240 [km s^-1] / radius [kpc]
    * conversion factor [kpc s km^-1 Myr^-1]
42      # This is a constant tangential speed of 240km/s from 5kpc and outwards
43      # and a linear increase from 0km/s to 240km/s for the innermost galaxy
44
45      # 0.00102271202633587 is the conversion factor from km/s to kpc/Myr
46      for coord in coordinates:
47          if coord[0]<5:
48              coord[1] += timestep * 0.00102271202633587 * 48
49              coord[1] %= 2 * np.pi
50          else:
51              coord[1] += timestep * 0.00102271202633587 * (240/coord[0])
52              coord[1] %= 2 * np.pi
53      return coordinates
54
55
56  def diffuse(coordinates, timestep, diffusion_constant=0.1):
57      # This diffuses the matter in the galaxy
58
59      old_coordinates = copy.deepcopy(coordinates)
60      for index, coord in enumerate(old_coordinates):
61          # consider each pixel in the galaxy, one by one
62          if coord[2] > 0:
63              # remove the matter already in the pixel
64              coordinates[index][2] -= coord[2]
65
66              # choose all points within diffusion distance to a pixel
67              # diffusion distance is calculated such:
68              #     diffusion distance [kpc] = sqrt(diffusion constant [kpc^2 Gyr
    ^-1] * timestep [Myr] * 0.001 [Gyr/Myr])
69              nearby_points = nearest_points(coord, old_coordinates, np.sqrt(
    diffusion_constant * timestep / 1000))
70
```

```python
71              # divide the matter in the pixel among the points determined to be
       nearby
72              avg_value = coord[2] / len(nearby_points)
73              for nb_point in nearby_points:
74                  coordinates[nb_point][2] += avg_value
75      return coordinates
76
77
78  def nearest_points(source_coord, coordinate_list, dist):
79      # calculates a straight line distance between pixels
80      # using the distance formula in polar coordinates
81      d = np.sqrt(source_coord[0] ** 2 + coordinate_list[:, 0] ** 2
82                  - 2 * source_coord[0] * coordinate_list[:, 0]
83                  * np.cos(source_coord[1] - coordinate_list[:, 1]))
84      # return list of points closer to the source pixel than a distance
85      nearby_points = np.where(d < dist)
86      return list(nearby_points[0])
87
88
89  def make_sources(coordinates, timestep, ns_list, current_iter, rate=24.1):
90      # This chooses some pixels to host a new NSM event
91
92      # the number of new NSM events is determined by the rate
93      no_ns = round(rate * timestep)
94      chosen_indices = np.random.randint(0, len(coordinates) - 1, no_ns)
95      for index in chosen_indices:
96          # for each NSM event add 100 arbitrary units of matter
97          coordinates[index][2] += 100.
98          new_ns = [current_iter, coordinates[index][0], coordinates[index][1]]
99          ns_list.append(new_ns)
100     # This returns the modified galaxy and a log file
101     return coordinates, ns_list
102
103
104 def save_galaxy(coordinates, name):
105     # This saves the data so they can be accessed later
106
107     # save an image of the galaxy with histogram attached
108     fig, ax = plt.subplots(ncols=2)
109     x = [0] * len(coordinates)
```

```python
110     y = [0] * len(coordinates)
111     colour = [0] * len(coordinates)
112     hist_data = [0] * len(coordinates)
113     for i in range(len(coordinates)):
114         hist_data[i] = coordinates[i][2]
115         if coordinates[i][2] != 0:
116             x[i] = coordinates[i][0] * np.sin(coordinates[i][1])
117             y[i] = coordinates[i][0] * np.cos(coordinates[i][1])
118             colour[i] = coordinates[i][2]
119     ax[0].scatter(x, y, c=colour, cmap='gray_r')
120     ax[0].scatter(0, 0, edgecolors='r', marker='x')
121     ax[0].set(adjustable='box', aspect='equal')
122     ax[0].set_xlim(-21, 21)
123     ax[0].set_ylim(-21, 21)
124     ax[1].hist(colour)
125     plt.tight_layout()
126     imagename = '.'.join((name, 'jpg'))
127     plt.savefig(imagename)
128     plt.close('all')
129
130     # save the data as a .csv file
131     dataname = '.'.join((name, 'csv'))
132     np.savetxt(dataname, coordinates, delimiter=',')
133
134
135 if __name__ == '__main__':
136     # the parameters that can be changed
137     inner_radius = 1
138     outer_radius = 20
139     radius_step = 0.06
140     timestep = 50
141     no_iterations = 250
142     diffusion_distance = 0.1
143
144     # make initial blank galaxy, setup folders and initialise
145     coord_list = make_galaxy(inner_radius, outer_radius, radius_step)
146     source = 'D:/xenon_data/precalculated/new set'
147     save_place = 'radius_step = {}/timestep = {}/construct'.format(radius_step,
        timestep)
148     folder = os.path.normpath(os.path.join(source, save_place, 'construct_7'))
```

```python
149     if not os.path.isdir(folder):
150         os.makedirs(folder)
151     ns_list = []
152     times_list = []
153
154     for i in range(no_iterations):
155         iter_name = os.path.join(folder, 'i={}'.format(i))
156
157         # add the new NSM sources
158         coord_list, ns_list = make_sources(coord_list, timestep, ns_list, i)
159
160         # diffuse the matter
161         coord_list = diffuse(coord_list, timestep, diffusion_distance)
162
163         # rotate the galaxy
164         rotate_galaxy(coord_list, timestep)
165
166         # save the data
167         save_galaxy(coord_list, iter_name, 'data')
168
169         # update the log file for the next iteration
170         log_name = os.path.join(folder, 'log.csv')
171         np.savetxt(log_name, ns_list, delimiter=',')
```

Attached below is the code used to analyse the model.

```python
import numpy as np
import os
import matplotlib.pyplot as plt




def rotate_source(source, angular_offset):
    for source_pixel in source:
        source_pixel[1] += angular_offset
        source_pixel[1] %= 2 * np.pi
    return source




def take_frac_difference(target_coords, removing_coords):
    # This identifies the corresponding pixels and then takes a fractional
    difference between them

    # initialise
    radii = list(set(target_coords[:,0]))
    radii.sort()
    output_list = []
    for radius in radii:
        # split the galaxy into rings
        target_ring = target_coords[np.where(target_coords[:,0] == radius)[0]]
        remove_ring = removing_coords[np.where(removing_coords[:, 0] == radius)
    [0]]
        output_ring = []
        for count, pixel in enumerate(target_ring):
            # split the ring into pixels
            output_pixel = pixel
            if count == 0:
                # find the corresponding pixel in the second galaxy for an
    initial pixel in the first galaxy
                position_offset, remove_pixel = take_closest(remove_ring, pixel
    [0], pixel[1])
                output_pixel[2] = abs((output_pixel[2] - remove_pixel[2])/
    output_pixel[2])
```

```python
35             else:
36                 # iterate through the ring
37                 # no need to recalculate the corresponding pixel each time
38                 wrapped_offset = (position_offset + count) % (len(target_ring) -
   1)
39                 output_pixel[2] = (output_pixel[2] - remove_ring[wrapped_offset
   ,2])/output_pixel[2]
40
41             output_ring.append(output_pixel)
42         output_list.extend(output_ring)
43     return np.array(output_list)
44
45
46 def take_closest(full_list, chosen_radius, chosen_angle):
47     # This chooses the pixel closest to the chosen coordinates
48     angular_dist = 10.
49     saved_item = []
50     saved_pos = 0
51     for pos, item in enumerate(full_list):
52         if (item[0] == chosen_radius) and (abs(chosen_angle - (item[1] % (2 * np
   .pi))) < angular_dist):
53             angular_dist = abs(chosen_angle - (item[1] % (2 * np.pi)))
54             saved_item = item
55             saved_pos = pos
56
57     return saved_pos, saved_item
58
59
60 def above_fraction(source_path, data_source, max_time, start_times, gap,
   frac_change):
61     # This calculates the fraction of pixels that have a fractional change
   greater than the predetermined 'frac_change'
62
63     # initialise
64     save_folder = os.path.join(source_path, 'analysis', data_source, 'fractional
    change', 'gap={}'.format(gap))
65     source_folder = os.path.join(source_path, data_source)
66     if not os.path.isdir(save_folder):
67         os.makedirs(save_folder)
68     data_file = '{}\\above {}.csv'.format(save_folder, frac_change)
```

```python
69      overall_change_data = []
70      plot_data = []
71
72      for start in start_times:
73          end = start + gap
74          if end > max_time:
75              continue
76
77          # load initial file and rotate it to correct for how the galaxy rotated
    between the times
78          start_file = os.path.join(source_path, data_source, 'i={}.csv'.format(
    start))
79          start_data = np.loadtxt(os.path.join(source_folder, start_file),
    delimiter=',')
80          start_data = rotate_galaxy(start_data, 0.1, float(end - start))
81
82          # load the final file
83          end_file = os.path.join(source_path, data_source, 'i={}.csv'.format(end)
    )
84          end_data = np.loadtxt(os.path.join(source_folder, end_file), delimiter='
    ,')
85
86          # find the fractional difference between the corresponding pixels
    between the two files
87          change_data = take_frac_difference(end_data, start_data)
88
89          # choose only the data between 5kpc and 15kpc
90          #     to exclude edge effects
91          cutoff_data = change_data[np.where((15 >= change_data[:, 0]) &
92                                              (5 <= change_data[:, 0]))]
93
94          # choose the pixels that fit the conditions
95          chosen_data = cutoff_data[np.where(frac_change <= cutoff_data[:, 2])]
96          cumulative_frac = len(chosen_data) / len(cutoff_data)
97
98          overall_change_data.append([start, cumulative_frac])
99          plot_data.append([start, cumulative_frac])
100     overall_change_data.sort()
101
102     # save the data
```

```python
103    np.savetxt('{}\\above {}.csv'.format(save_folder, frac_change, start_times
       [0]), overall_change_data,
104               delimiter=',')
105    print(overall_change_data)
106    fig = plt.figure()
107    x = np.zeros(len(plot_data))
108    y = np.zeros(len(plot_data))
109    cumulative_x = 0
110    cumulative_y = 0
111    for i in range(len(plot_data)):
112        x[i] = plot_data[i][0]
113        y[i] = plot_data[i][1]
114    plt.plot(x, y)
115    plt.savefig('{}\\above {} ({}-{}).jpg'.format(save_folder, frac_change,
       start_times[0], start_times[-1]))
116    plt.close()
117
118
119
120 def track_sun(source_path, data_source, index=60000):
121    # This tracks the matter in a pixel
122    # the index is chosen so that the pixel is roughly 8.34kpc from the centre
123
124    # initialisation
125    output_folder = os.path.join(source_path, 'analysis', data_source, 'track
       sun')
126    if not os.path.exists(output_folder):
127        os.makedirs(output_folder)
128    file_list = os.listdir(os.path.join(source_path,data_source))
129    output_list = []
130
131    for file in file_list:
132        if '.csv' in file:
133            if 'log' in file:
134                continue
135            # extract the file name
136            path = os.path.join(source_path, data_source, file)
137            name = int(file.split('.csv')[0].split('=')[1])
138            coordinates = np.loadtxt(path, delimiter=',')
139            if file == 'i=0.csv':
```

```python
                initial_pos = [coordinates[index][0], coordinates[index][1]]
            output_data = [int(name), float(coordinates[index][2])]
            output_list.append(output_data)
    output_list.sort()


    # save the data and make a figure
    output_file_name = os.path.join(output_folder, '{:.2f}, {:.2f}'.format(
    initial_pos[0], initial_pos[1]))
    np.savetxt('{}.csv'.format(output_file_name), output_list, delimiter=',')
    plot_data = np.loadtxt('{}.csv'.format(output_file_name), output_list,
    delimiter=',')
    plt.plot(plot_data)
    plt.savefig('{}.jpg'.format(output_file_name))
    plt.close()
```